AD A051646

ODC FILE COPY

AFML-TR-77-144

11

CHARACTERIZATION OF COMPOSITE LAMINATES USING TUBULAR SPECIMENS

MECHANICS AND SURFACE INTERACTIONS BRANCH
NONMETALLIC MATERIALS DIVISION

AUGUST 1977

TECHNICAL REPORT AFML-TR-77-144
Interim Report for Period 1 January 1976 — 1 December 1976

Approved for public release; distribution unlimited.

AIR FORCE MATERIALS LABORATORY
AIR FORCE WRIGHT AERONAUTICAL LABORATORIES
AIR FORCE SYSTEMS COMMAND
WRIGHT-PATTERSON AIR FORCE BASE, OHIO 45433

NOTICE

When Government drawings, specifications, or other data are used for any purpose other than in connection with a definitely related Government procurement operation, the United States Government thereby incurs no responsibility nor any obligation whatsoever; and the fact that the government may have formulated, furnished, or in any way supplied the said drawings, specifications, or other data, is not to be regarded by implication or otherwise as in any manner licensing the holder or any other person or corporation, or conveying any rights or permission to manufacture, use, or sell any patented invention that may in any way be related thereto.

This report has been reviewed by the Information Office (OI) and is releasable to the National Technical Information Service (NTIS). At NTIS, it will be available to the general public, including foreign nations.

This technical report has been reviewed and is approved for publication.

Stephen W. Tsai

Stephen W. Tsai
Project Engineer

FOR THE DIRECTOR

Stephen W. Tsai

Stephen W. Tsai, Chief
Mechanics and Surface Interactions Branch
Nonmetallic Materials Division

Copies of this report should not be returned unless return is required by security considerations, contractual obligations, or notice on a specific document.

AIR FORCE/56780/26 January 1978 — 250

(9) Technical Rept. 1 Jan - 1 Dec 76

UNCLASSIFIED

SECURITY CLASSIFICATION OF THIS PAGE (When Data Entered)

REPORT DOCUMENTATION PAGE

READ INSTRUCTIONS BEFORE COMPLETING FORM

1. REPORT NUMBER: (14) AFML-TR-77-144 ✓

2. GOVT ACCESSION NO.

3. RECIPIENT'S CATALOG NUMBER

4. TITLE (and Subtitle): (6) Characterization of Composite Laminates Using Tubular Specimens.

5. TYPE OF REPORT & PERIOD COVERED: Jan 1, 1976 - Dec 1, 1976

6. PERFORMING ORG. REPORT NUMBER

7. AUTHOR(s): (10) H.T./Hahn, J./Erikson

8. CONTRACT OR GRANT NUMBER(s)

9. PERFORMING ORGANIZATION NAME AND ADDRESS:
Air Force Materials Laboratory (AFML/MBM)
Air Force Wright Aeronautical Laboratories
Wright-Patterson AFB, Ohio 45433

10. PROGRAM ELEMENT, PROJECT, TASK AREA & WORK UNIT NUMBERS: 2307P1 (16) 2307 (17) P1

11. CONTROLLING OFFICE NAME AND ADDRESS: (11)
Air Force Materials Laboratory (AFML/MBM)
Air Force Wright Aeronautical Laboratories
Wright-Patterson AFB, Ohio 45433

12. REPORT DATE: Aug[illegible]977 (12) 54p.

13. NUMBER OF PAGES: 48

14. MONITORING AGENCY NAME & ADDRESS (if different from Controlling Office)

15. SECURITY CLASS. (of this report): Unclassified

15a. DECLASSIFICATION/DOWNGRADING SCHEDULE

16. DISTRIBUTION STATEMENT (of this Report)

Approved for public release, distribution unlimited.

17. DISTRIBUTION STATEMENT (of the abstract entered in Block 20, if different from Report)

Approved for public release, distribution unlimited.

18. SUPPLEMENTARY NOTES

19. KEY WORDS (Continue on reverse side if necessary and identify by block number)

Graphite/Epoxy	Failure Surface
Compliances	Combined Loading
Tubular Specimens	Symmetry of Elasticity Tensor
Failure Criterion	Compression Modulus

20. ABSTRACT (Continue on reverse side if necessary and identify by block number)

Properties of a unidirectional graphite/epoxy (T300/5208) composite are characterized using tubular specimens. The elastic compliances based on the average invariants are found to describe fairly accurately the elastic behavior under various combined loadings. The equality between the tension and compression compliances and the symmetry of the compliance tensor are also established to within the experimental scatter. The matrix/interface-controlled failure is characterized by a second-order polynomial including a over

DD FORM 1473, 1 JAN 73 EDITION OF 1 NOV 65 IS OBSOLETE

UNCLASSIFIED

SECURITY CLASSIFICATION OF THIS PAGE (When Data Entered)

012 3..

20. (Abstract)

first-order term. This failure criterion agrees with the experimental observation that the compressive loading perpendicular to the fibers can increase the longitudinal shear stress required for failure.

FOREWORD

This report was prepared in the Mechanics and Surface Interactions Branch (AFML/MBM), Nonmetallic Materials Division, Air Force Materials Laboratory, Wright-Patterson AFB, Ohio. The work was performed under the support of Project No. 2307 "Aerospace Sciences," Task No. 2307P1 "Life Analysis and Failure Mechanics in Engine and Airframe Structural Metals and Composites." The time period covered by the effort was 1 January 1976 to 1 December 1976. Stephen W. Tsai (AFML/MBM) was the laboratory project engineer and J. Erikson was a visiting scientist from the National Defense Research Institute, Stockholm, Sweden.

The authors wish to acknowledge R. Y. Kim, R. Esterline, and R. Cornwell of the University of Dayton Research Institute for the preparation and testing of composite tubular specimens.

TABLE OF CONTENTS

SECTION		PAGE
I	INTRODUCTION	1
II	EXPERIMENTAL PROCEDURE	3
	1. Specimens	3
	2. Test Procedure	3
III	RESULTS AND ANALYSIS	5
	1. Elastic Compliances	5
	2. Elastic Behavior Under Combined Loadings	8
	3. Strength	8
IV	CONCLUSTIONS	12
	REFERENCES	13

LIST OF ILLUSTRATIONS

FIGURE		PAGE
1	Reference Coordinate Systems	22
2	Photomicrograph of $[0]_{8T}$ Tube	23
3	Tube with Grips Attached at Ends	24
4	Dimensions of Grip	25
5	Compliances Measured in Axial Loading: (a) $S'^{(+)}_{11}$ versus $S'^{(-)}_{11}$; (b) $-S'^{(+)}_{21}$ versus $-S'^{(-)}_{21}$; (c) $S'^{(+)}_{61}$ versus $S'^{(-)}_{61}$	26-28
6	Compliances Measured in Torsional Loading: (a) $S'^{(+)}_{16}$ versus $S'^{(-)}_{16}$; (b) $S'^{(+)}_{26}$ versus $S'^{(-)}_{26}$; (c) $S'^{(+)}_{66}$ versus $S'^{(-)}_{66}$	29-31
7	S'_{61} versus S'_{16}	32
8	Compliance Invariants..............................	33
9	Off-Axis Compliances: (a) S'_{11}; (b) S'_{12}; (c) S'_{16}; (d) S'_{26}; (e) S'_{66}	34-38
10	Analysis-Experiment Correlation: (a) $\lvert\epsilon_x/\sigma_x\rvert$; (b) $\lvert\epsilon_y/\sigma_x\rvert$; (c) $\lvert\epsilon_{xy}/\sigma_x\rvert$; (d) $\lvert\epsilon_x/\sigma_{xy}\rvert$; (e) $\lvert\epsilon_y/\sigma_{xy}\rvert$; (f) $\lvert\epsilon_{xy}/\sigma_{xy}\rvert$	39-44
11	Failure Surface in $\sigma_2 - \sigma_6$ Plane	45
12	Distribution of f	46
13	Effect of Longitudinal Stress on f	47
14	Failure Modes of Composite Tubes	48

LIST OF TABLES

TABLE		PAGE
1	Tube Dimensions	15
2	Elastic Compliances	16
3	Parameters a and b	18
4	Average Invariants and Average Compliances	19
5	Stress Ratios in Combined Loadings	20
6	Stress Components at Failure	21

SECTION I

INTRODUCTION

Composite tube has attracted attention as a possible specimen geometry because it offers several advantages over straight-sided coupons. One of the advantages is that it can provide data under combined loading conditions. As a corollary to this, the effect of end constraints commonly observed in off-axis tests [1] can be eliminated. In case of angle-ply laminates a tube is not subject to the so-called free edge effects [2] which cannot be avoided in coupon specimens.

Furthermore, the need for testing under a combined state of stress arises if one wants to answer some of the basic questions such as the symmetry of the elastic tensor [3], the equality of the tension and compression moduli [4], and the interaction between the transverse and shear stress components in the matrix/interface-controlled failure [5].

In spite of the aforementioned advantages and needs, the available data from tubular specimens is rather minimal, the main reason being the high cost of fabricating and testing tubes of high quality.

Another problem associated with tubular specimens of anisotropic material is that the uniformity of the state of stress produced depends on the anisotropy as well as the geometry. Tube dimensions required to achieve a uniform state of stress have been studied both analytically and theoretically [6-12]. Although the exact geometry depends on the material properties, it has been found that the gage section should be at least twice as long as the diameter and that the wall thickness-to diameter ratio should be less than 0.03 to ensure fairly uniform stress distribution. Typical tube dimensions reported in the literature are listed in Table 1. The tubular specimens tested in the present study have the same dimensions as none of these. However, they satisfy the minimum requirements aforementioned.

The present report presents results from the combined loading tests of off-axis, unidirectional composite tubes. The data are then analyzed in such a way as to answer the questions raised above regarding the material properties. It is hoped that the amount of data gathered is sufficient to infer statistically meaningful conclusions.

SECTION II

EXPERIMENTAL PROCEDURE

1. SPECIMENS

Specimens are unidirectional 8-ply graphite/epoxy (T300/5208) tubes 30.5 cm long and 4.06 cm in outside diameter. Each tube is identified by the fiber orientation angle followed by a specimen number. Thus the specimen -45-2, for example, is one of the $[-45]_{8T}$ tubes. The reference coordinate systems used to define the fiber orientation angle θ is shown in Figure 1, where x is parallel to the tube axis and 1 is the fiber direction. The tubes were purchased from the Whittaker Corp. and had been kept in the room environment until the test. This waiting period was long enough to allow equilibrium moisture content in the tubes.

The fiber volume content was found to be 58 ± 5% from the photomicrographs of a $[0]_{8T}$ tube. Examination of the photomicrographs also revealed that the material had unusually large void content ranging up to 2.1%. The voids manifest themselves in the low transverse strength, as discussed later. Figure 2 is a photomicrograph showing a void.

2. TEST PROCEDURE

Six pairs of end fixtures were made to grip the tubes. A tube with a grip attached at each end is shown in Figure 3. The grip essentially consists of two concentric cylinders, Figure 4. The gap between these two cylinders is filled with an adhesive material and then a tube specimen is slipped in. The adhesive is a mixture of Epon 828 (6 parts) and Versamid (4 parts). The complete setup was cured for one hour at 93°C.

All tests were performed on an MTS closed loop testing system which is fully computerized. The loading rate ranged approximately from 0.5 to 5 MPa/s and strains were measured at the middle of the gage section using the three-element (0/45/90) strain rosettes (Micro-Measurements Type

EA-06-125RD-350). The stress-strain measurements were taken at 20 equal intervals up to the maximum applied stresses and were stored in the computer memory. The data were analyzed immediately after each test. The following procedure was adopted to calculate the elastic compliances.

Suppose ϵ and σ are the strain and stress component, respectively, of interest. Then the paired data $\left\{\epsilon^{(i)}, \sigma^{(i)} \mid i = 1, 2, \cdots, 20\right\}$ were fit by a linear equation of the form

$$\epsilon^{(i)} = S\sigma^{(i)} + d$$

The average slope S, which is the elastic compliance, was then printed out on the printer.

In all, four different types of tests were performed to characterize the elastic properties:

1. Axial loading - tension ($\sigma_x > 0$) and compression ($\sigma_x < 0$)
2. Torsional loading - positive ($\sigma_{xy} > 0$) and negative ($\sigma_{xy} < 0$)
3. Positive combined loading ($\sigma_{xy}/\sigma_x > 0$) - ($\sigma_x > 0, \sigma_{xy} > 0$) and ($\sigma_x < 0$, $\sigma_{xy} < 0$)
4. Negative combined loading ($\sigma_{xy}/\sigma_x < 0$) - ($\sigma_x > 0$, $\sigma_{xy} < 0$) and ($\sigma_x < 0$, $\sigma_{xy} > 0$)

SECTION III

RESULTS AND ANALYSIS

1. ELASTIC COMPLIANCES

Elastic compliances measured from the tubes are summarized in Table 2. In all cases the same tension-compression and pure torsion in both directions were repeated three times, so that the number of measurements analyzed is 24 for each specimen. It should be noted that one test consists of loading and unloading, thus providing two measurements of the same compliance. The compliances are defined by the following equations:

$$e_x = S'_{11}\sigma_x + S'_{16}\sigma_{xy} , \tag{1}$$

$$e_y = S'_{21}\sigma_x + S'_{26}\sigma_{xy} , \tag{2}$$

$$e_{xy} = S'_{61}\sigma_x + S'_{66}\sigma_{xy} , \tag{3}$$

Here, the subscripts x and y are the reference coordinates for loading, Figure 1.

For 0-degree tubes S'_{16}, S'_{61}, and S'_{26} should vanish since the material is orthotropic. The measurements are not exactly as predicted theoretically; however, the data show large scatter, indicating that the nonzero values are probably a result of experimental error as well as of the deviation from the assumed uniform state of stress.

Unusually high coefficient of variation (C.V.) in S'_{21} and S'_{26} of speciment 15-3 is due to the large difference between tension and compression moduli which is in turn believed to result from the poor alignment.

In order to check the equality of compliance under loadings in opposite directions, e.g. tension and compression, $S'^{(+)}_{ij}$ are plotted against $S'^{(-)}_{ij}$ in Figures 5 and 6. The superscripts (+) and (-) denote the compliances obtained under positive and negative loadings, respectively. In these figures the solid lines are the linear least squares fit of the data. That is,

the data were fit by an equation of the form

$$S'^{(+)}_{ij} = aS'^{(-)}_{ij} + b \quad , \tag{4}$$

and the corresponding parameters a and b are listed in Table 3, together with the coefficient of correlation r. In plotting the data absolute values were used when $S'^{(+)}_{ij}$ and $S'^{(-)}_{ij}$ have the same sign; otherwise, the actual measurements, including sign, were plotted, e.g. Figure 5(c).

Figures 5 show that the compliances measured in simple tension and compression are equal to each other except for S'_{21}. $|S'_{21}|$ is seen from Figure 5(b) to be slightly higher in tension than in compression. It is interesting to note that $|S'_{21}|$ tends to be larger in tension for the off-axis angles $|\theta| \geq 45^o$ and smaller in tension when $|\theta| < 45^o$.

Figures 6 similarly show that the compliances measured in torsion are independent of whether the torque is positive or negative. Here the positive torque is defined to be in the same direction as is the angle θ. Thus, the positive torque results in a positive torsional stress ($\sigma_{xy}>0$) if θ is positive and in a negative torsional stress ($\sigma_{xy}<0$) if θ is negative.

The best-fit line in Figure 6(b) indicates that $S'^{(-)}_{26}$ is slightly lower than $S'^{(+)}_{26}$. However, the three points far off to the right are from the specimen which exhibited appreciable misalignment. Although how this misalignment affects the compliance is not exactly known, it is suspected that the deviation is due to the misalignment. Thus, if we neglect these measurements, the results will undoubtedly improve the equality between $S'^{(+)}_{26}$ and $S'^{(-)}_{26}$.

Average values of S'_{61} are plotted against average values of S'_{16} in Figure 7 to check the symmetry requirements. The data are from Table 2. For the material tested, the deviation from the symmetry is rather small.

Averaging of the compliance data can be performed by using the invariants [13, 14]. The necessary invariants are

$$I_1 = (S'_{11} + S'_{22} + 2S'_{12}) / 4 \tag{5}$$

$$I_2 = (S'_{11} + S'_{22} - 2S'_{12} + S'_{66}) / 8 \tag{6}$$

$$R_1 = \left[(-S'_{11} + S'_{22})^2 + (S'_{16} + S'_{26})^2\right]^{1/2} / 2 \tag{7}$$

$$R_2 = \left[(S'_{11} + S'_{22} - 2S'_{12} - S'_{66})^2 + 4(S'_{26} - S'_{16})^2\right]^{1/2} / 8 \tag{8}$$

In the above equations S'_{16} stands for the average of S'_{16} and S'_{61} in Table 2.

The calculated invariants are shown in Figure 8. The mean values of the invariants and the corresponding coefficients of variation are listed in Table 4. The invariants I_1 and R_2 show higher scatter than do the invariants I_2 and R_1. In the calculation it was assumed that

$$S'_{22}(\theta) = S'_{11}(90 - \theta)$$

because S'_{22} was not measured, and that $S'_{16} = S'_{26} = 0$ for 0- and 90-deg. specimens.

The average invariants are then used to calculate the compliances through the equations

$$\overline{S}_{11} = \overline{I}_1 + \overline{I}_2 - \overline{R}_1 - \overline{R}_2 \tag{9}$$

$$\overline{S}_{22} = \overline{I}_1 + \overline{I}_2 + \overline{R}_1 - \overline{R}_2 \tag{10}$$

$$\overline{S}_{12} = \overline{I}_1 - \overline{I}_2 + \overline{R}_2 \tag{11}$$

$$\overline{S}_{66} = 4\overline{I}_2 + 4\overline{R}_2 , \tag{12}$$

where an over bar denotes average. The resulting compliances are also listed in Table 4.

Comparison between the predictions from the average compliances and the off-axis data is shown in Figures 9. Aside from the experimental scatter, the curves based on the average compliances are in fairly good agreement with the data.

2. ELASTIC BEHAVIOR UNDER COMBINED LOADINGS

The stress ratios employed in the combined loading tests are listed in Table 5. These tests can serve as a check on how sufficiently the average compliances describe the elastic behavior. The loading paths in the $\sigma_x - \sigma_{xy}$ plane have been described in Section II. The resulting strain-to-stress ratios are then analytically determined from

$$e_x/\sigma_x = S'_{11} + S'_{16}\sigma_{xy}/\sigma_x \quad (13)$$

$$e_y/\sigma_x = S'_{12} + S'_{26}\sigma_{xy}/\sigma_x \quad (14)$$

$$e_{xy}/\sigma_x = S'_{16} + S'_{66}\sigma_{xy}/\sigma_x \quad (15)$$

$$e_x/\sigma_{xy} = S'_{11}\sigma_x/\sigma_{xy} + S'_{16} \quad (16)$$

$$e_y/\sigma_{xy} = S'_{12}\sigma_x/\sigma_{xy} + S'_{26} \quad (17)$$

$$e_{xy}/\sigma_{xy} = S'_{16}\sigma_x/\sigma_{xy} + S'_{66} \quad (18)$$

In Figures 10 the calculated values are on the abscissa and the measured ones on the ordinate. The straight lines in the figures represent a perfect correlation. In all cases, the data are scattered closely around these lines, indicating a good correlation.

3. STRENGTH

The stress components along the material symmetry axes at failure are listed in Table 6. As mentioned before, these stresses are introduced by applying the axial stress σ_x and the torsional stress σ_{xy} simultaneously while keeping the ratio σ_{xy}/σ_x constant.

If any coupling between the fiber failure and the matrix/interface failure is neglected, then the matrix/interface failure criterion can be written as

$$f(\sigma_2, \sigma_6) = F_2\sigma_2 + F_{22}\sigma_2^2 + F_{66}\sigma_6^2 = 1 \qquad (19)$$

The strength tensor components F_2, F_{22}, and F_{66} are then determined by the linear least squares method:

$$[\sigma]^T [\sigma] \{F\} = [\sigma]^T \{1\} \qquad (20)$$

where

$$[\sigma] = \begin{bmatrix} \sigma_2^{(1)} & \sigma_2^{(1)^2} & \sigma_6^{(1)^2} \\ \sigma_2^{(2)} & \sigma_2^{(2)^2} & \sigma_6^{(2)^2} \\ - & - & - \\ \sigma_2^{(n)} & \sigma_2^{(n)^2} & \sigma_6^{(n)^2} \end{bmatrix} \qquad (21)$$

$$\{F\} = \begin{Bmatrix} F_2 \\ F_{22} \\ F_{66} \end{Bmatrix} \qquad (22)$$

and $\{1\}$ is the 1 x n column matrix whose elements are all unity. The superscript (i) stands for the i-th data set. Note that the total number of measurements, n, is 26 in the present case. The results are

$$F_2 = 3.376 \times 10^{-2} \, (\mathrm{MPa})^{-1}$$

$$F_{22} = 4.721 \times 10^{-4} \, (\mathrm{MPa})^{-2}$$

$$F_{66} = 2.384 \times 10^{-4} \, (\mathrm{MPa})^{-2}$$

The corresponding failure surface in the σ_2 - σ_6 plane is shown in Figure 11.

Table 6 lists the value of f calculated for each tube from the above F's and the failure stresses. Since the minimum value of f is less than zero, i.e.

$$f_{min} = -\frac{F_2^2}{4F_{22}} = -0.6035 \tag{23}$$

the scatter of f is fit by a Weibull distribution of the following form:

$$R = \exp\left[-\left(\frac{f-f_{min}}{\hat{f}}\right)^{\alpha}\right] \tag{24}$$

R is the probability of the failure function greater than f. The shape and scale parameters determined are

$$\alpha = 3.055 \quad , \quad \hat{f} = 1.5265$$

and the coefficient of correlation is 0.9729.

The average value of f obtained from the distribution (24) is only 0.76, which is much lower than the unity initially assumed. This is also apparent in Figure 12 where there are more data points inside the failure surface ($f < 1$) than outside ($f > 1$). The reason is because the least squares fit places more weight on the higher stresses through second order terms in the polynomial. Thus lower stresses have less influence on the strength tensor components.

The effect of the longitudinal stress component on the matrix/interface failure is studied in Figure 13 by plotting the value of f at failure against σ_1. The coefficient of correlation for the data is only 0.0306, indicating very little influence of σ_1 on the matrix/interface failure within the range of σ_1 applied. Note that the maximum σ_1 is less than 30% of the typical longitudinal strength.

Now that the failure function is known, one can examine the margin of safety involved in the elastic property tests. The maximum value of f to be reached in each test can be calculated by substituting the intended terminal stress components in the failure function. The results are listed in Tables 2 and 5. In Table 2, f_x and f_{xy} are the maximum values of f in the axial and torsional tests, respectively, and the superscripts (+) and (-) in Table 5 stand for the sign of σ_{xy}/σ_x.

Comparison of the values of f in the elastic tests with those at failure reveals that two specimens, -15-2 and 60-2, did not fail in the combined elastic tests although in theory they should have failed; i.e., the maximum f was exceeded in both cases. Thus, it may be concluded that the value of f at failure depends on the state of stress, which is contrary to the assumed failure criterion. However, in all the other cases, failure did not occur, as expected, when f was less than that at failure. This indicates that the discrepancy in the two cases mentioned above is probably due to the variation from specimen to specimen of the strength tensor components.

In all the tests, failure initiated in the test section in the form of cracking along the fibers. Typical failure modes are shown in Figure 14 for every off-axis angle tested. Multiple fracture of 60-deg specimens is a result of those specimens not being able to sustain much torque after the fracture.

SECTION IV

CONCLUSIONS

Elastic compliances and the matrix/interface-controlled failure surface of a unidirectional graphite/epoxy composite (T300/5208) have been determined by testing off-axis tubular specimens. Invariants have been used to obtain the average compliances and the linear least squares method to determine the failure surface.

A good agreement is shown between the prediction and the data for the elastic behavior under combined loadings. The equality between the tension and compression compliances and the symmetry of the compliance tensor are established to within the experimental scatter.

The failure surface in the σ_2 - σ_6 plane is characterized by a second-order polynomial including a first-order term in σ_2. This failure criterion agrees with the experimental observation that the compressive loading perpendicular to the fibers can increase the longitudinal shear stress required for failure (See [5] for Gr/Ep, [10] for B/Ep, and [15] for Gl/Ep). This is not surprising if one notes that the matrix/interface-controlled failure initiates from the inherent defects, such as voids and partial debond, which are aligned fairly parallel to the fibers.

Unfortunately, a large scatter is seen in the strength data and furthermore the transverse strengths, both tensile and compressive, calculated from the strength tensor are lower than what are reported in the literature. This difference is believed to be due to the unusually high void content detected in the specimens used. However, the data still show the common failure characteristics expected of graphite/epoxy composites.

REFERENCES

1. N. J. Pagano and J. C. Halpin, "Influence of End Constraint in the Testing of Anisotropic Bodies," J. Composite Materials, Vol. 2 (1968), p. 18.

2. R. B. Pipes and N. J. Pagano, "Interlaminar Stresses in Composite Laminates Under Uniform Axial Extension," J. Composite Materials, Vol. 4 (1970), p. 538.

3. C. W. Bert and T. R. Guess, "Mechanical Behavior of Carbon/Carbon Filamentary Composites," Composite Materials: Testing and Design (Second Conf.), ASTM STP 497, 1972, p. 89.

4. R. M. Jones, "Mechanics of Composite Materials with Different Moduli in Tension and Compression," Mechanics of Composites Review, Air Force Materials Laboratory and Air Force Office of Scientific Research, Oct. 1976.

5. E. M. Wu, "Phenomenological Anisotropic Failure Criterion," Composite Materials, Vol. 2, Mechanics of Composite Materials, G. P. Sendeckyj, Ed., 1974, p. 353.

6. N. J. Pagano and J. M. Whitney, "Geometric Design of Composite Cylindrical Characterization Specimens," J. Composite Materials, Vol. 4(1970), p. 360.

7. R. R. Rizzo and A. A. Vicario, "A Finite Element Analysis for Stress Distribution in Gripped Tubular Specimens," Composite Materials: Testing and Design (Second Conf), ASTM STP 497, 1972, p. 68.

8. E. M. Wu, "Optimal Experimental Measurements of Anisotropic Failure Tensors," J. Composite Materials, Vol. 6(1972), p. 473.

9. R. S. Sandhu, et al, Laminate Tubular Specimens Subjected to Biaxial Stress State, AFFDL-TR-73-7 Vol. 1 & 2, Air Force Flight Dynamics Laboratory, Feb. 1973 and Mar. 1975.

10. B. W. Cole and R. B. Pipes, Filamentary Composite Laminates Subjected to Biaxial Stress Fields, AFFDL-TR-73-115, Air Force Flight Dynamics Laboratory, June 1974.

11. G. C. Grimes, et al, An Experimental Investigation of the Stress Levels at which Significant Damage Occurs in Graphite Fiber Plastic Composites, AFML-TR-72-40, Air Force Materials Laboratory, May 1972.

12. T. L. Sullivan and C. C. Chamis, "Some Important Aspects in Testing High-Modulus Fiber Composite Tubes in Axial Tension," Analysis of the Test Methods for High Modulus Fibers and Composites, ASTM STP 521, 1973, p. 277.

13. E. M. Wu, K. L. Jerina, and R. E. Lavengood, "Data Averaging of Anisotropic Material Constants," Analysis of Test Methods for High-Modulus Fibers and Composites, ASTM STP 521, 1973, p. 229.

14. S. W. Tsai and H. T. Hahn, Composite Materials Workbook, AFML-TR-77-33, Air Force Materials Laboratory, March 1977.

15. U. Hutter, H. Schelling, and H. Krauss, "An Experimental Study to Determine Failure Envelope of Composite Materials with Tubular Specimens Under Combined Loads and Comparison Between Several Classical Criteria," AGARD-CP-163, AGARD Conf. Proc. No. 163, NATO, March 1975.

TABLE 1. TUBE DIMENSIONS

Material	Length cm(in)	Diameter cm(in)	Thickness mm(in)	Gage Length cm(in)	Reference
Gr/Ep	12.7(5)	2.54(1)	1.27(0.05)	7.62(3)	[8]
Gl/Ep & Gr/Ep	33.0(13)	10.2(4)	1.27(0.05)	10.2(4)	[9]
B/Ep	25.4(10)	10.2(4)	0.76-1.52 (0.03-0.06)	10.2(4)	[10]
Gr/Ep	25.4(10)	2.54(1)	1.02-2.41 (0.04-0.095)	10.2(4)	[11]
Gl/Ep & Gr/Ep	30.5(12)	5.08(2)	1.52(0.06)	25.4(10)	[12]
Carbon/ Carbon	—	7.62(3)	3.18(0.125)	7.62(3)	[3]

TABLE 2. ELASTIC COMPLIANCES

SPEC. NO.		S'_{11} $(TPa)^{-1}$	$-S'_{21}$ $(TPa)^{-1}$	S'_{61} $(TPa)^{-1}$	S'_{16} $(TPa)^{-1}$	S'_{26} $(TPa)^{-1}$	S'_{66} $(TPa)^{-1}$	f_x	f_{xy}
0-2	Ave.	7.423	2.129	1.955	4.859	-3.137	151.43	0	.05
	C.V.(%)	5.76	7.62	165.4	31.5	31.8	1.55		
0-3	Ave.	8.047	2.158	-0.059	0.325	3.401	149.04	0	.05
	C.V.(%)	3.48	9.24	1553.0	40.3	47.0	2.18		
0-4	Ave.	8.090	2.435	0.361	0.928	1.069	154.30	0	.01
	C.V.(%)	17.8	6.06	216.5	20.6	27.1	3.17		
15-1	Ave.	15.72	6.633	-31.79	-31.26	-3.764	139.77	.09	.29
	C.V.(%)	2.72	6.85	3.56	4.25	5.51	2.44		
-15-1	Ave.	19.42	3.408	44.40	37.59	14.36	172.25	.10	.56
	C.V.(%)	3.34	17.4	3.10	3.06	4.13	1.69		
-15-2	Ave.	16.16	6.151	35.20	32.52	14.46	135.75	.04	.13
	C.V.(%)	8.39	21.2	10.4	8.52	21.8	3.85		
-15-3	Ave.	17.88	5.564	38.58	33.40	9.409	150.84	.10	.13
	C.V.(%)	2.05	1.70	2.98	3.62	3.45	4.00		
15-3	Ave.	16.20	2.084	-40.96	-34.05	-29.46	172.88	.04	.13
	C.V.(%)	2.14	50.5	5.46	4.96	40.2	5.25		
-30-1	Ave.	41.13	11.16	51.68	49.15	26.79	120.50	.17	.48
	C.V.(%)	2.00	8.88	2.28	1.47	2.64	1.62		
-30-2	Ave.	43.18	8.740	49.92	49.54	31.53	117.54	.13	.22
	C.V.(%)	1.47	6.14	1.54	3.58	3.97	3.59		

TABLE 2. ELASTIC COMPLIANCES (Continued)

-30-3			Failure in torsion					.17	.48
-45-2	Ave.	72.87	13.47	55.59	52.08	50.59	125.07	.15	.56
	C.V.(%)	4.00	13.7	5.61	1.63	2.16	1.43		
-45-3	Ave.	71.36	6.039	39.33	42.68	45.05	113.43	.15	.26
	C.V.(%)	4.56	14.1	7.14	8.24	9.50	3.85		
-60-1	Ave.	87.17	1[illegible]67	35.33	35.68	51.13	131.35	.23	.48
	C.V.(%)	1.77	15.9	12.3	3.66	1.62	2.22		
60-2	Ave.	84.51	15.34	-21.87	-33.66	-46.18	129.66	.23	.22
	C.V.(%)	1.44	5.14	17.4	2.61	2.72	5.32		
-60-3	Ave.	90.15	11.59	34.13	28.46	45.95	135.64	.23	.22
	C.V.(%)	3.24	15.1	14.1	2.45	2.26	6.24		
90-1	Ave.	106.11	5.178	7.759	0.021	3.308	185.60	.31	.05
	C.V.(%)	2.58	25.8	55.4	6366	24.5	2.65		
90-2	Ave.	93.74	3.720	9.992	1.614	1.593	154.73	.31	.01
	C.V.(%)	1.32	3.61	42.3	32.6	11.4	2.74		
90-3	Ave.	99.70	3.691	9.774	2.580	4.109	162.62	.31	.01
	C.V.(%)	0.96	3.47	44.2	10.4	4.31	4.72		
90-4			Failure in tension					.31	.01
90-5	Ave.	98.73	5.587	5.846	1.539	3.580	160.61	.31	.01
	C.V.(%)	2.45	43.3	74.4	18.4	32.3	1.91		
90-6	Ave.	103.37	2.750	5.291	2.023	12.12	148.13	.31	.01
	C.V.(%)	1.32	9.86	30.9	35.8	22.8	3.07		

TABLE 3. PARAMETERS a and b

	S'_{11}	$-S'_{12}$	S'_{61}	S'_{16}	S'_{26}	S'_{66}	S'_{61} vs. S'_{16}
a	0.984	1.026	0.975	0.980	0.936	1.006	0.950
b, $(TPa)^{-1}$	0.945	0.333	0.412	0.065	-0.480	-0.611	3.497
r	0.9974	0.9152	0.9599	0.9930	0.9557	0.9595	0.9683

TABLE 4. AVERAGE INVARIANTS AND AVERAGE COMPLIANCES

	$\bar{I}_1$	$\bar{I}_2$	$\bar{R}_1$	$\bar{R}_2$
Ave., $(TPa)^{-1}$	26.43	34.63	46.22	5.510
C.V., %	8.96	5.29	5.49	17.50

$\bar{S}_{11}$ $(TPa)^{-1}$	$\bar{S}_{12}$ $(TPa)^{-1}$	$\bar{S}_{22}$ $(TPa)^{-1}$	$\bar{S}_{66}$ $(TPa)^{-1}$
9.33	-2.69	101.77	160.56

TABLE 5. STRESS RATIOS IN COMBINED LOADINGS

Spec. No.	σ_{xy} / σ_x	$f^{(+)}$	$f^{(-)}$
0 - 2	± 0.2	0.05	0.05
0 - 3	± 0.2	0.05	0.05
0 - 4	± 0.4	0.01	0.01
15 - 1	± 0.4	0.17	0.45
-15 - 1	± 0.5	0.24	0.38
-15 - 2	± 0.4	0.19	-0.07
-15 - 3	± 0.2	0.26	0.04
15 - 3*	± 0.4	.081	0.19
-30 - 1	± 0.8	0.72	0.29
-30 - 2	± 0.5	0.38	0.09
-45 - 2	± 1.67	0.76	0.37
-45 - 3	± 0.83	0.43	0.10
-60 - 1	± 1.67	0.77	0.24
60 - 2	± 0.83	0.48	0.02
-60 - 3	± 0.83	0.48	0.02
90 - 1	± 1.67	0.36	0.36
90 - 2	± 0.83	0.32	0.32
90 - 3	± 0.83	0.32	0.32
90 - 5	± 0.83	0.32	0.32
90 - 6	± 0.83	0.32	0.32

* Failure in negative loading.

TABLE 6. STRESS COMPONENTS AT FAILURE

Spec. No.	σ_1 MPa	σ_2 MPa	σ_6 MPa	f	Is σ_{xy}/σ_x the same as one of those in elastic tests?
0 - 1	375.4	0	44.38	0.470	-
0 - 2	0	0	48.04	0.550	Yes
0 - 3	-375.4	0	-39.02	0.363	Yes[a]
0 - 4	0	0	-48.60	0.563	Yes
15 - 1	-259.4	-18.62	59.50	0.687	Yes
-15 - 1	139.2	9.99	37.30	0.716	Yes
-15 - 2	135.1	-8.03	3.12	-0.238	No
-15 - 3	323.2	-58.68	-66.20	0.689	No
15 - 3	11.49	4.26	-9.50	0.174	Yes
-30 - 1	118.4	12.78	45.26	0.997	No
-30 - 2	193.8	-85.15	-17.79	0.623	No
-30 - 3	-11.64	11.61	6.69	0.466	Yes
-45 - 1	-13.79	25.03	5.62	1.148	-
-45 - 2	97.22	-97.22	0	1.180	Yes
-45 - 3	155.4	-85.81	34.78	0.867	No
-60 - 1	55.60	11.05	51.34	1.059	No
60 - 2	86.56	-34.81	-64.91	0.401	No
-60 - 3	116.1	-78.02	78.03	1.691	No
90 - 1	0	12.82	0	0.510	Yes
90 - 2	0	23.67	0	1.064	Yes
90 - 2'[b]	0	20.26	0	0.878	-
90 - 3	0	0	-74.95	1.339	Yes
90 - 3'[b]	0	0	-79.36	1.501	-
90 - 4	0	8.04	0	0.302	Yes
90 - 5	0	8.94	0	0.340	Yes
90 - 6	0	0	70.12	1.172	Yes

a. Influence of σ_1 is neglected.

b. Retested after failure.

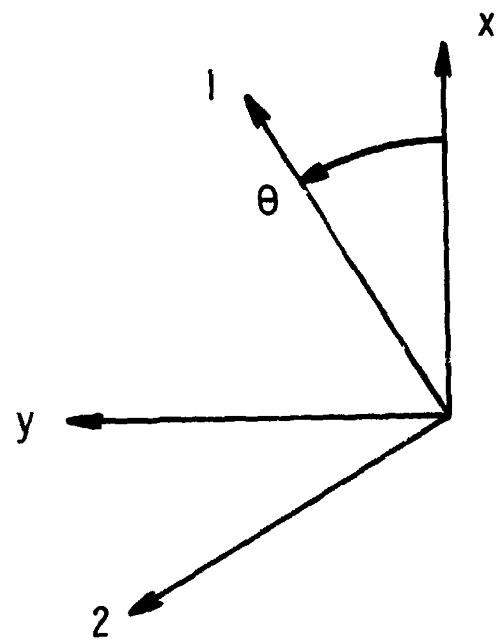

Figure 1. Reference Coordinate Systems

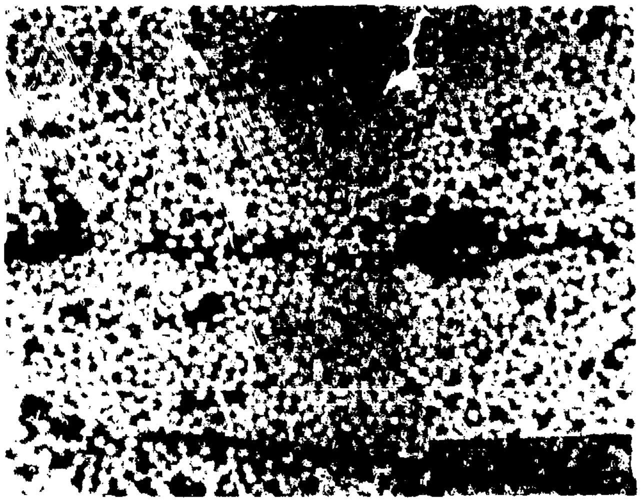

Figure 2. Photomicrograph of $[0]_{8T}$ Tube

Figure 3. Tube with Grips Attached at Ends

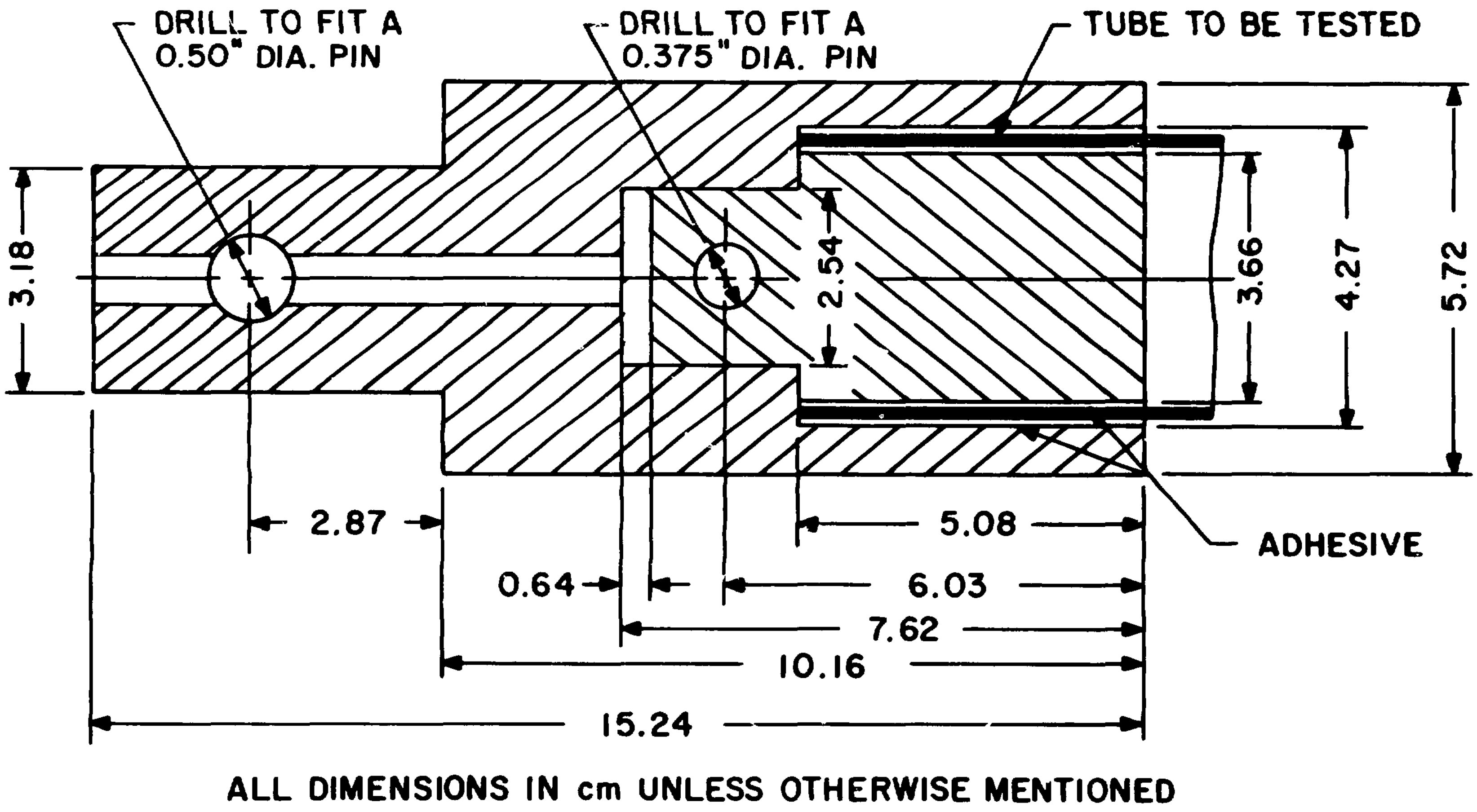

Figure 4. Dimensions of Grip

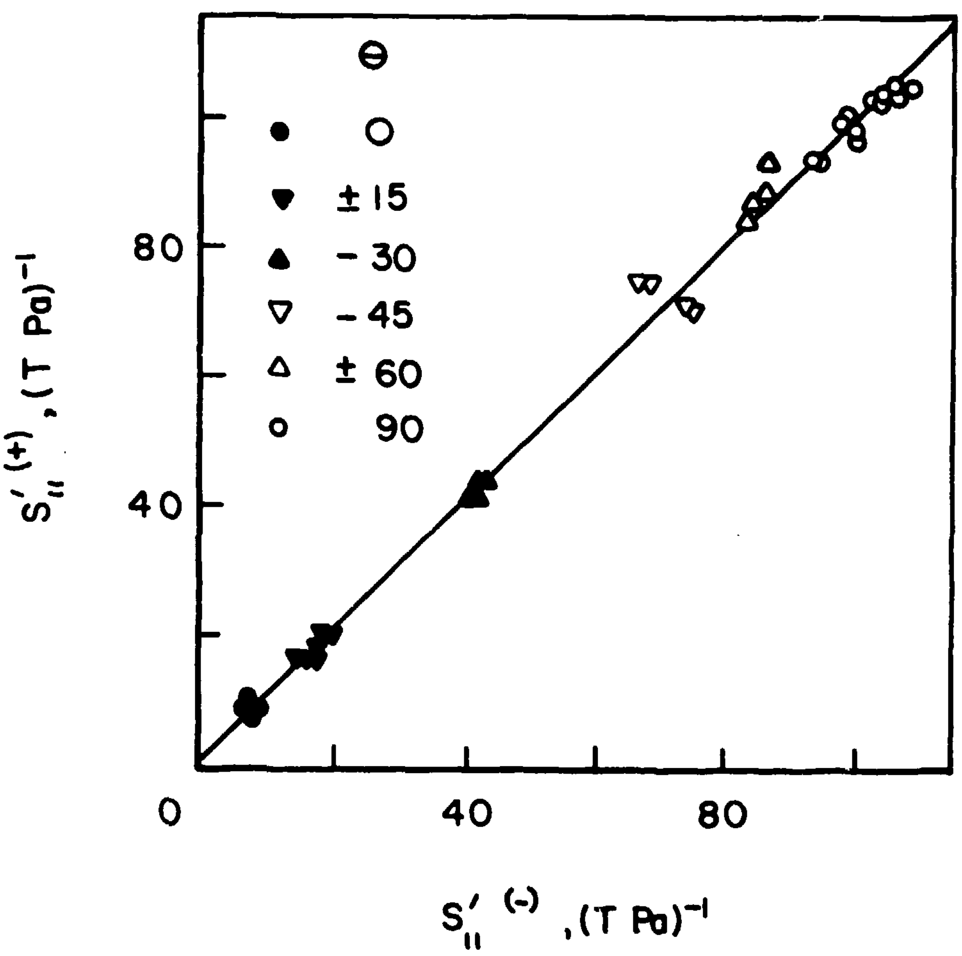

Figure 5. Compliances Measured in Axial Loading: (a) $S'^{(+)}_{11}$ versus $S'^{(-)}_{11}$

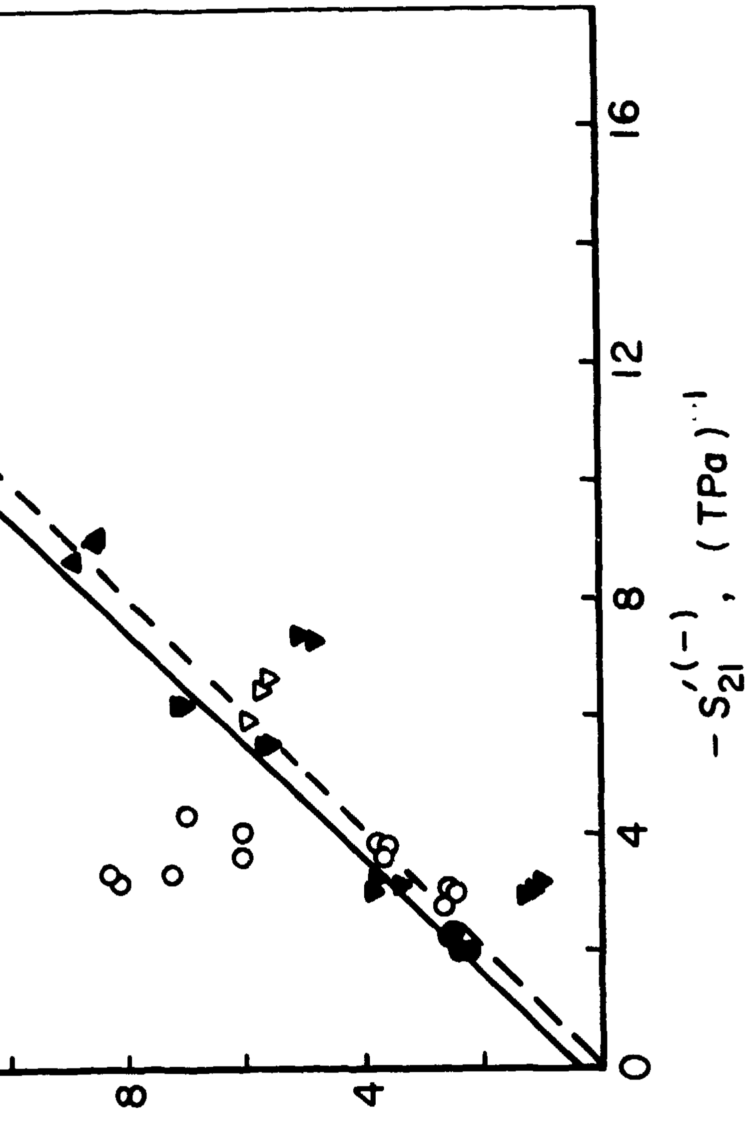

Figure 5(b). $-S_{21}^{\prime(+)}$ versus $-S_{21}^{\prime(-)}$

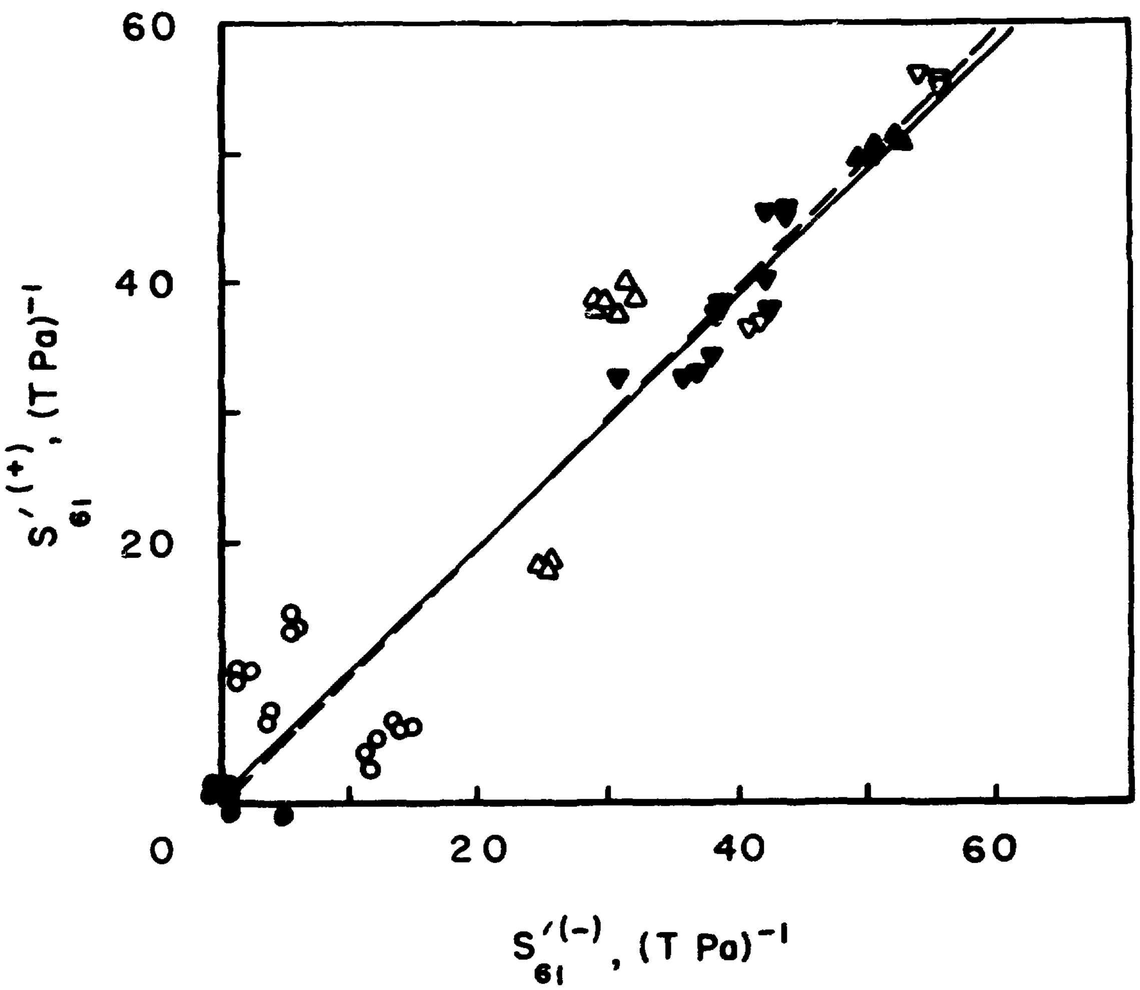

Figure 5(c). $S'^{(+)}_{61}$ versus $S'^{(-)}_{61}$

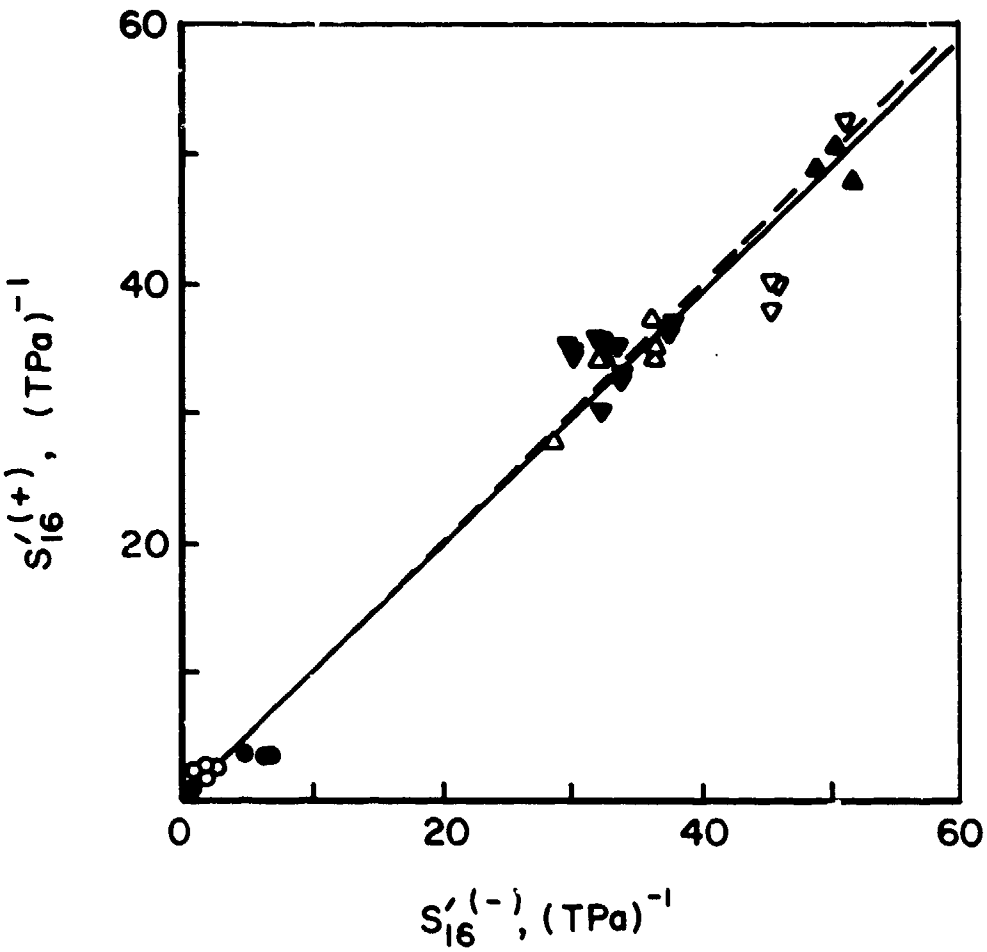

Figure 6. Compliances Measured in Torsional Loading:
(a) $S'^{(+)}_{16}$ versus $S'^{(-)}_{16}$

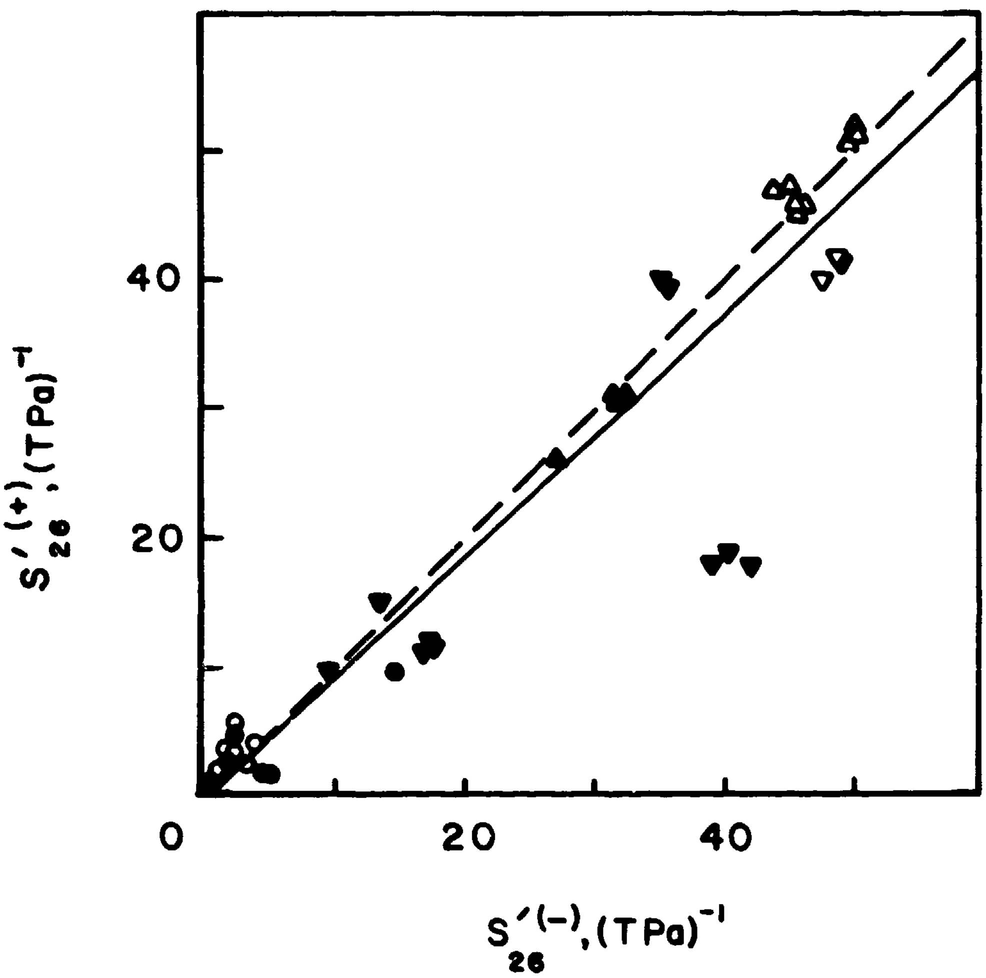

Figure 6(b). $S'^{(+)}_{26}$ versus $S'^{(-)}_{26}$

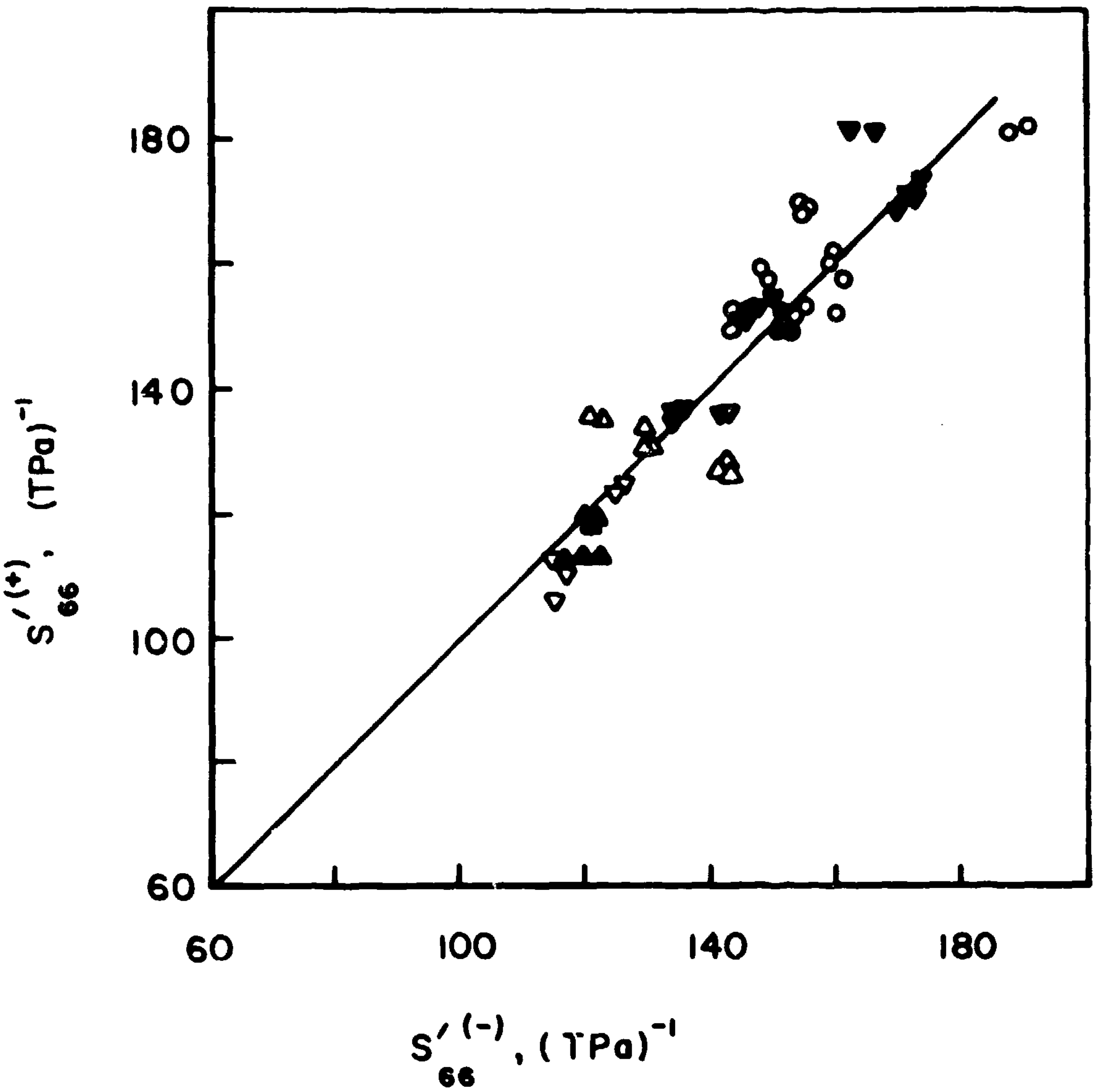

Figure 6(c). $S_{66}'^{(+)}$ versus $S_{66}'^{(-)}$

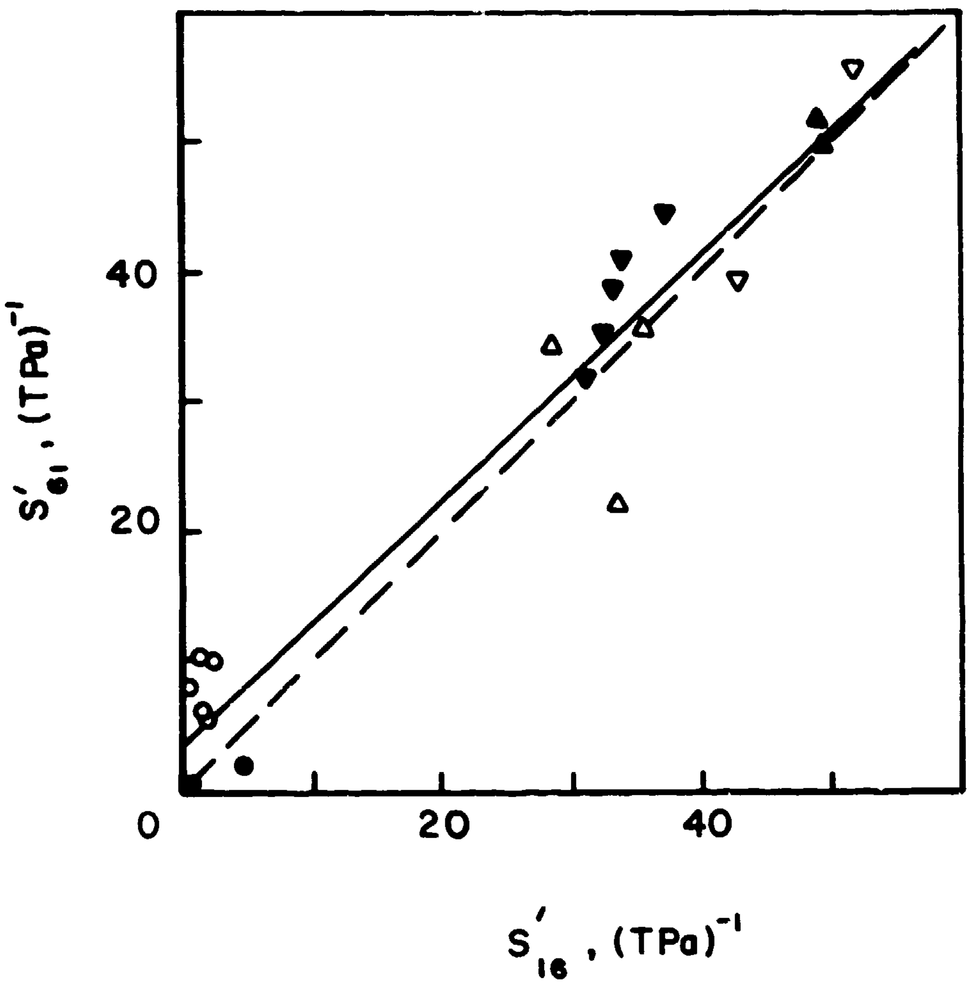

Figure 7. S'_{61} versus S'_{16}

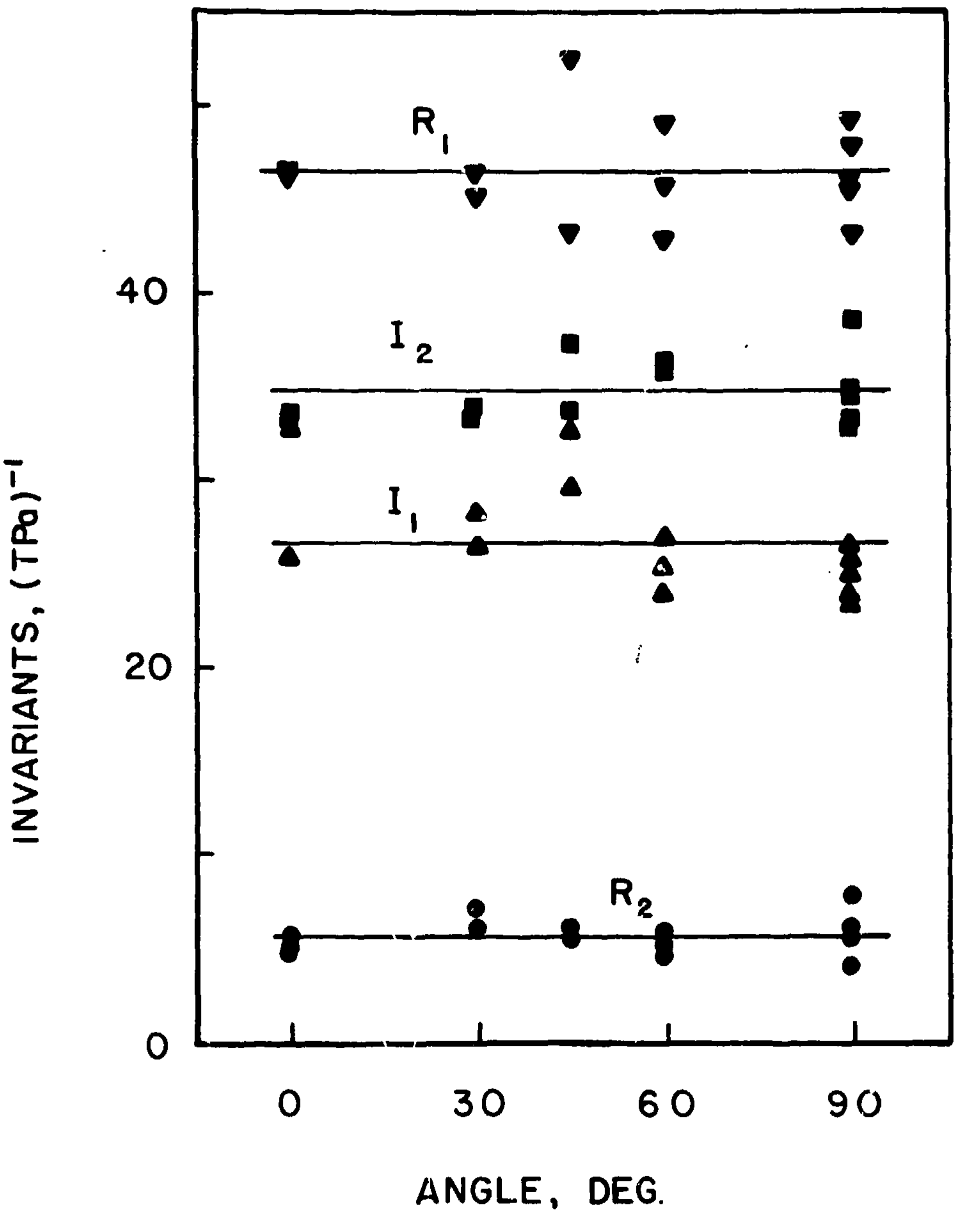

Figure 8. Compliance Invariants

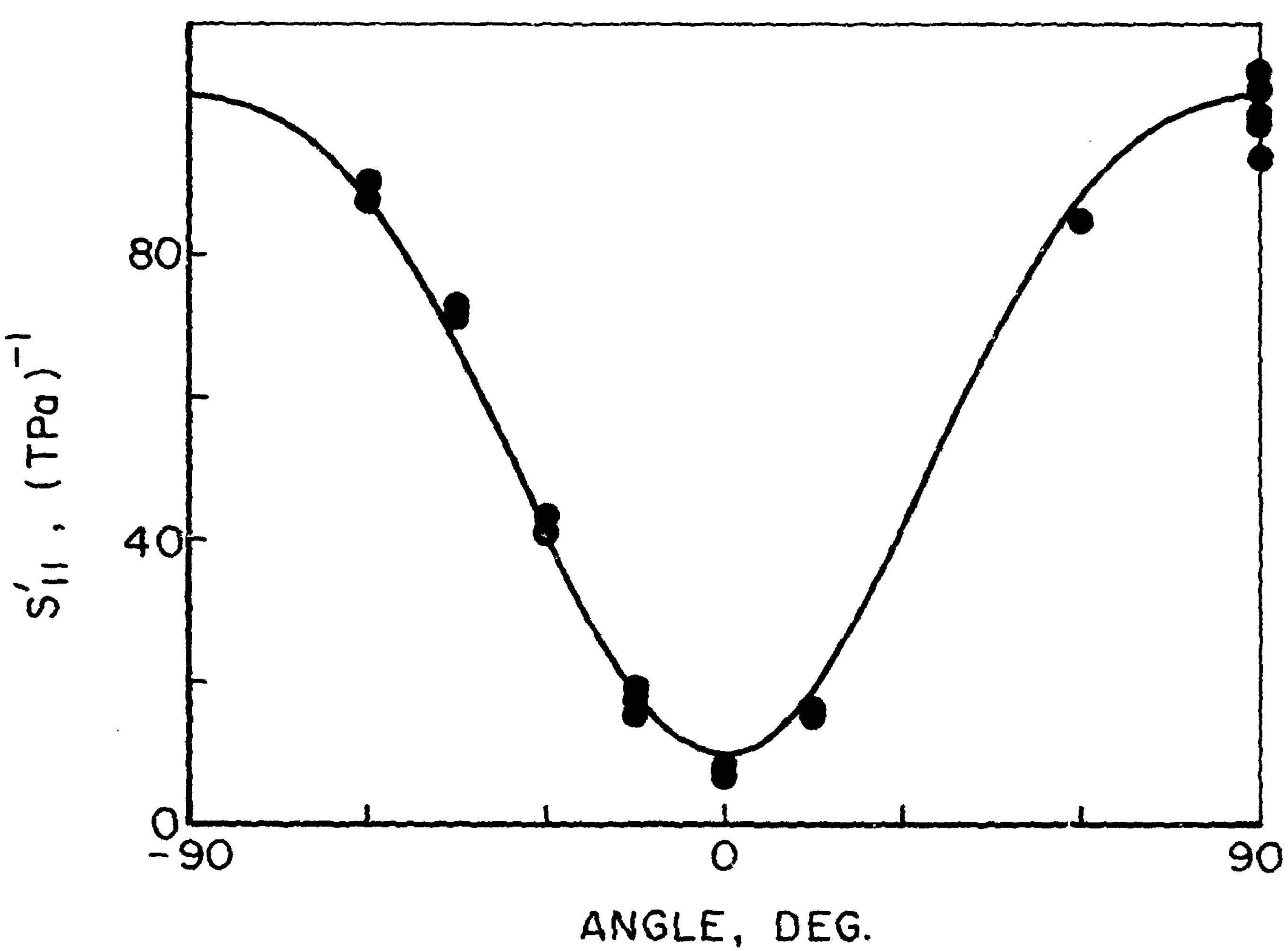

Figure 9. Off-Axis Compliances:
(a) S'_{11}

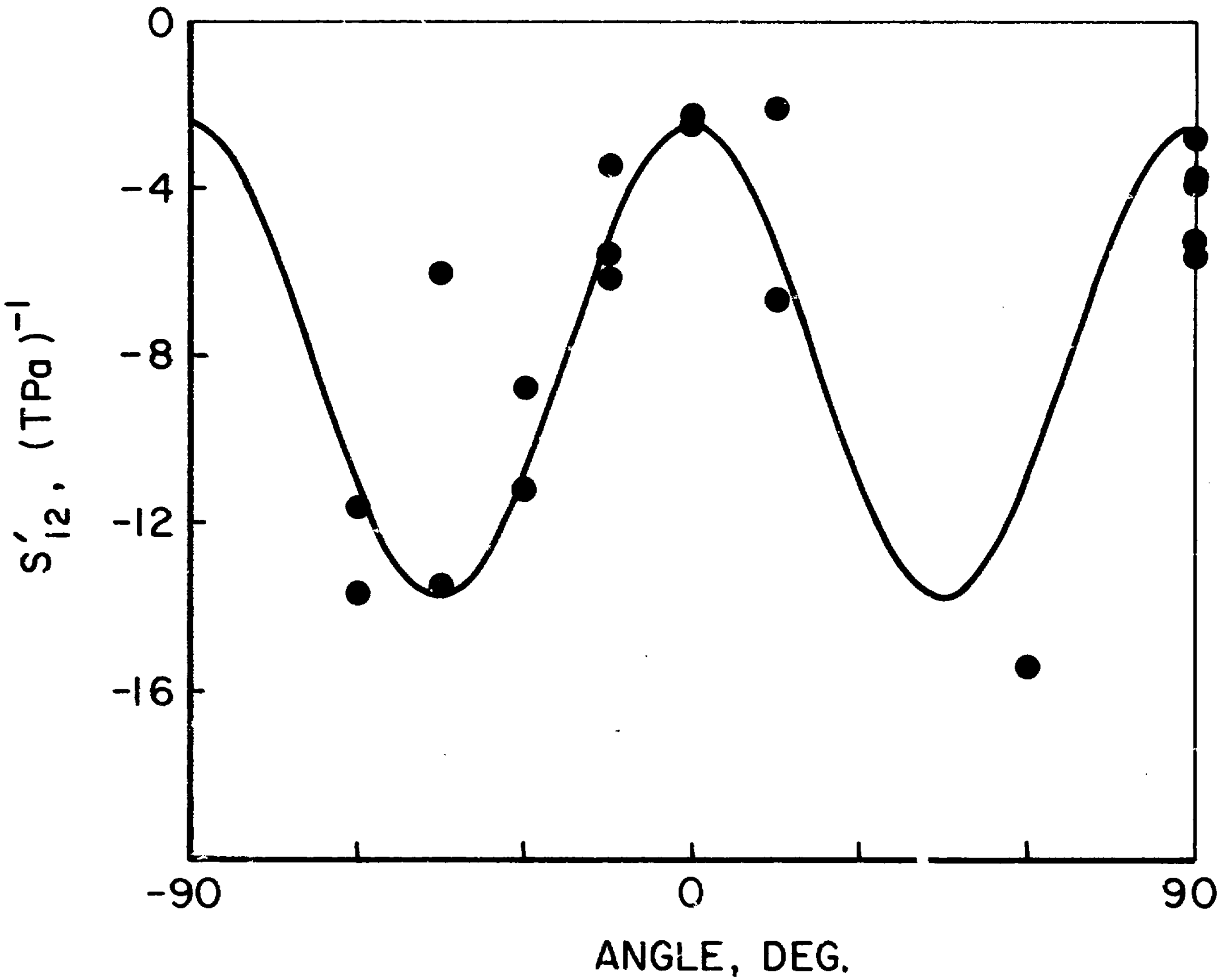

Figure 9(b). S'_{12}

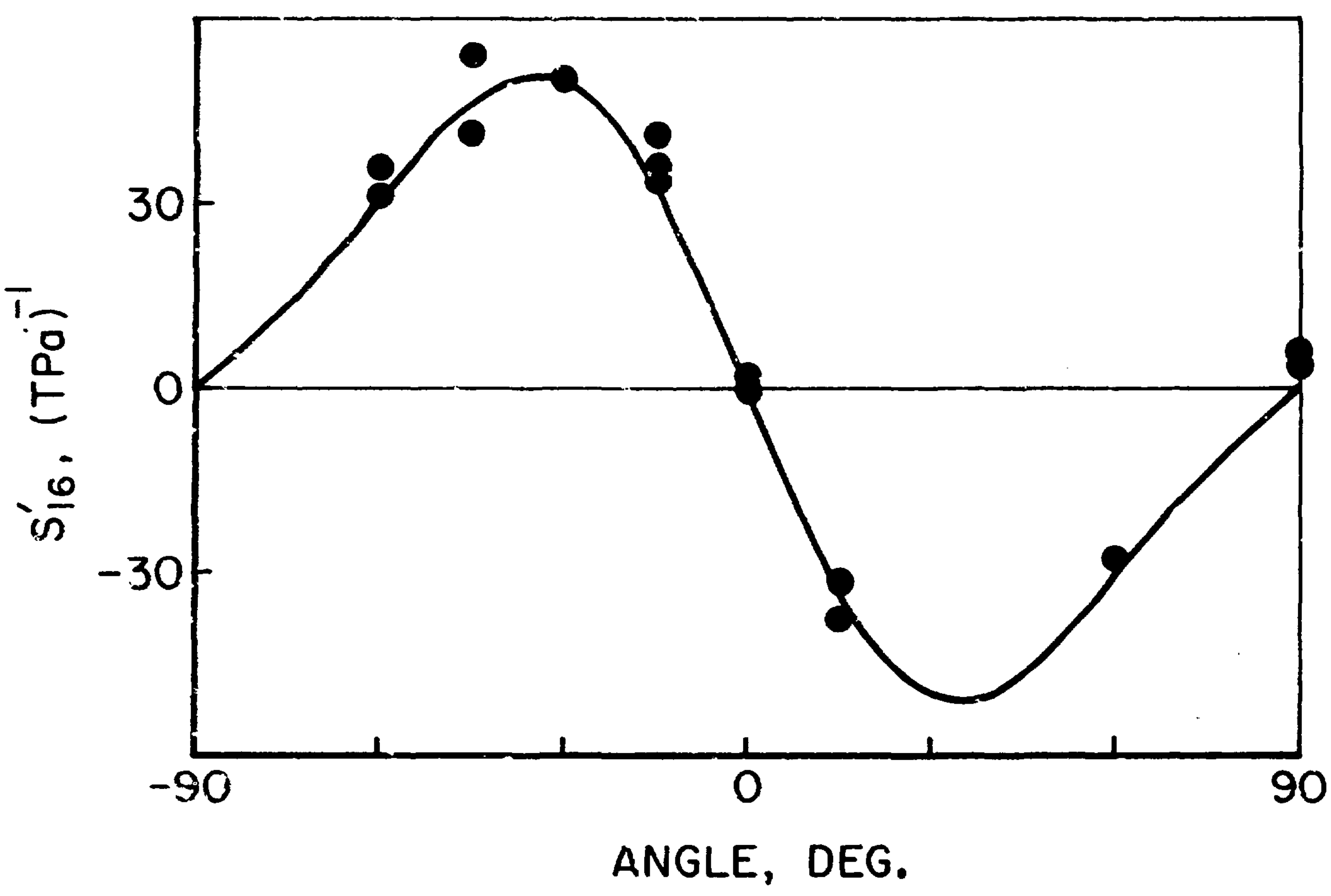

Figure 9(c). S'_{16}

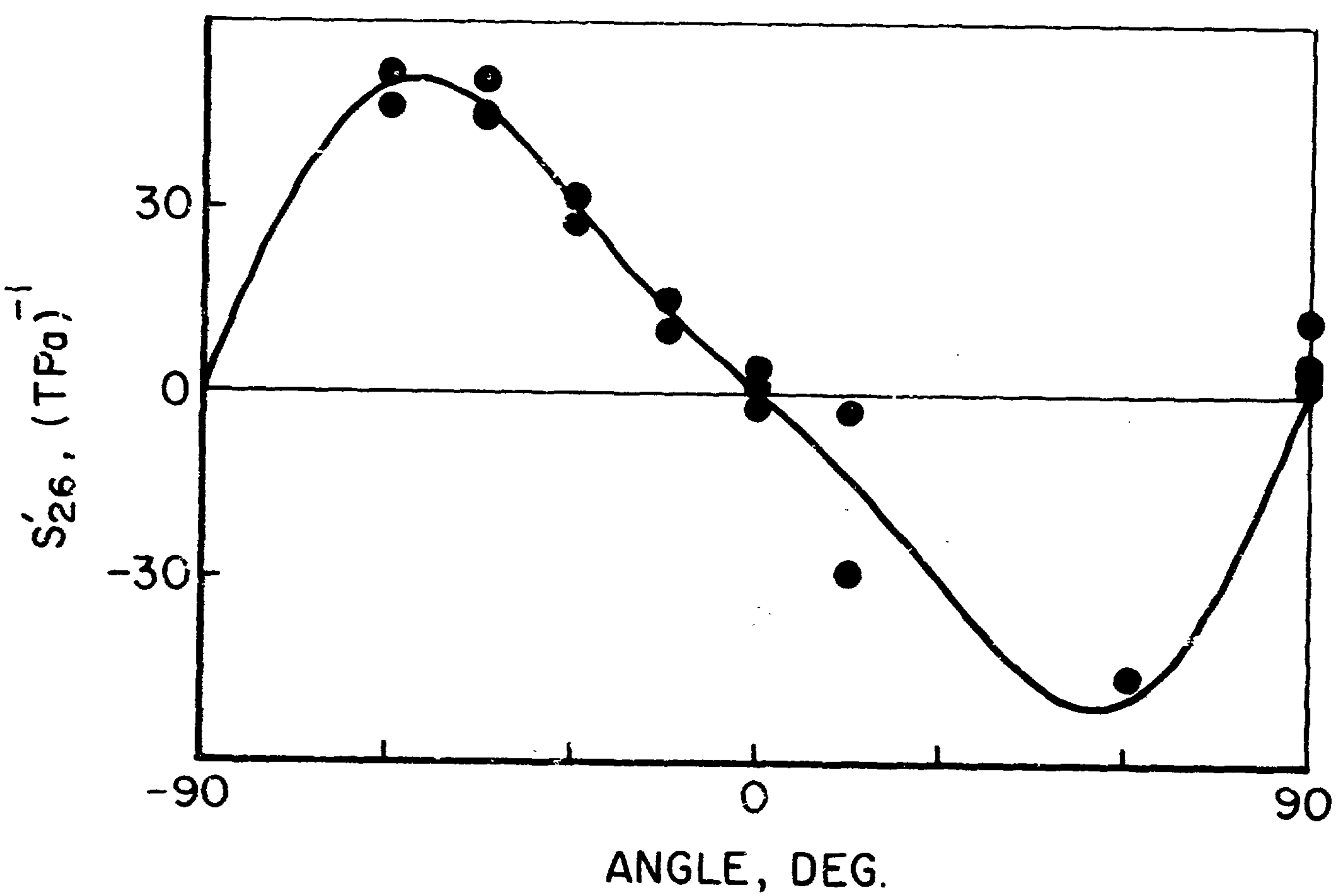

Figure 9(d). S'_{26}

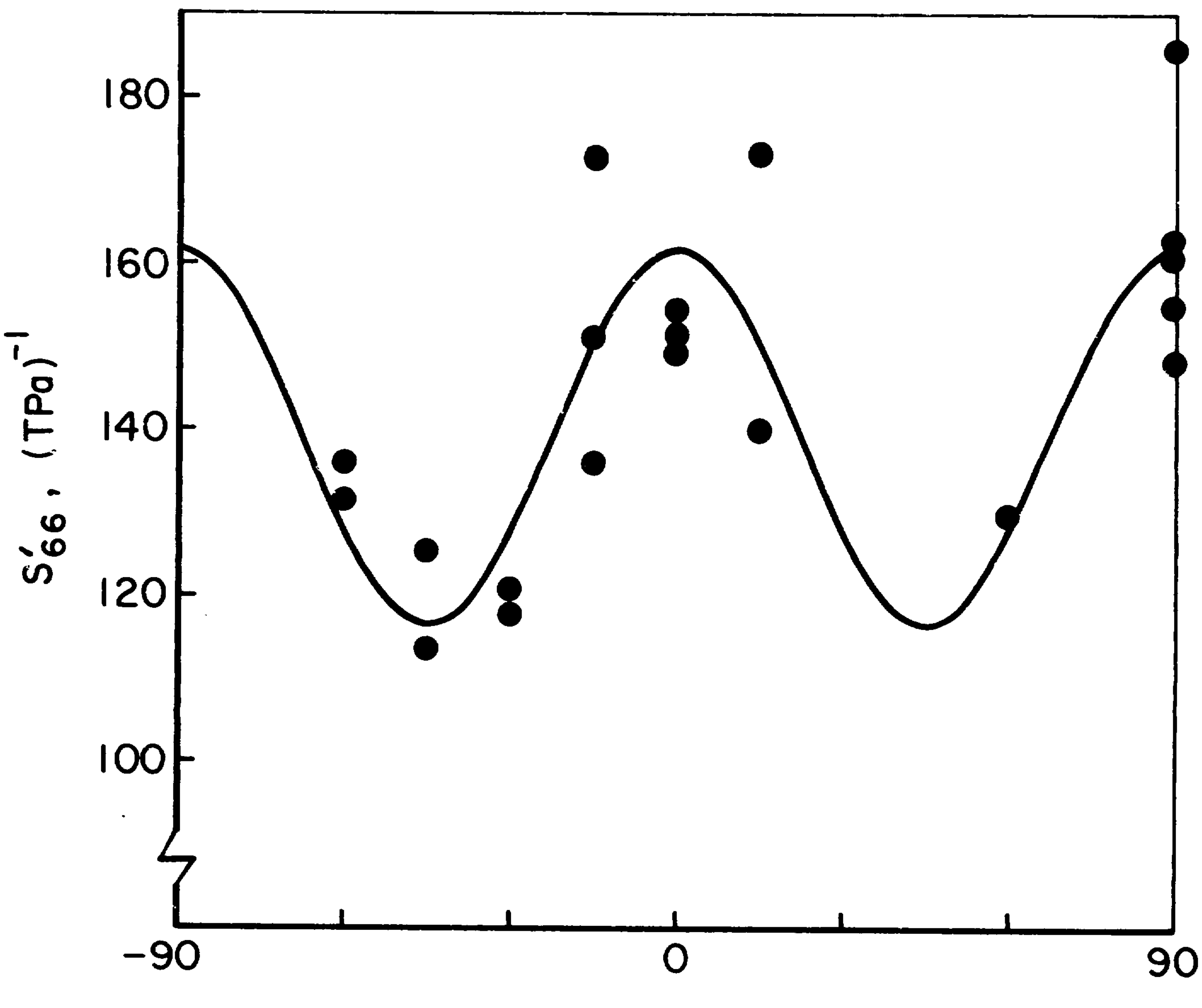

Figure 9(e). S'_{66}

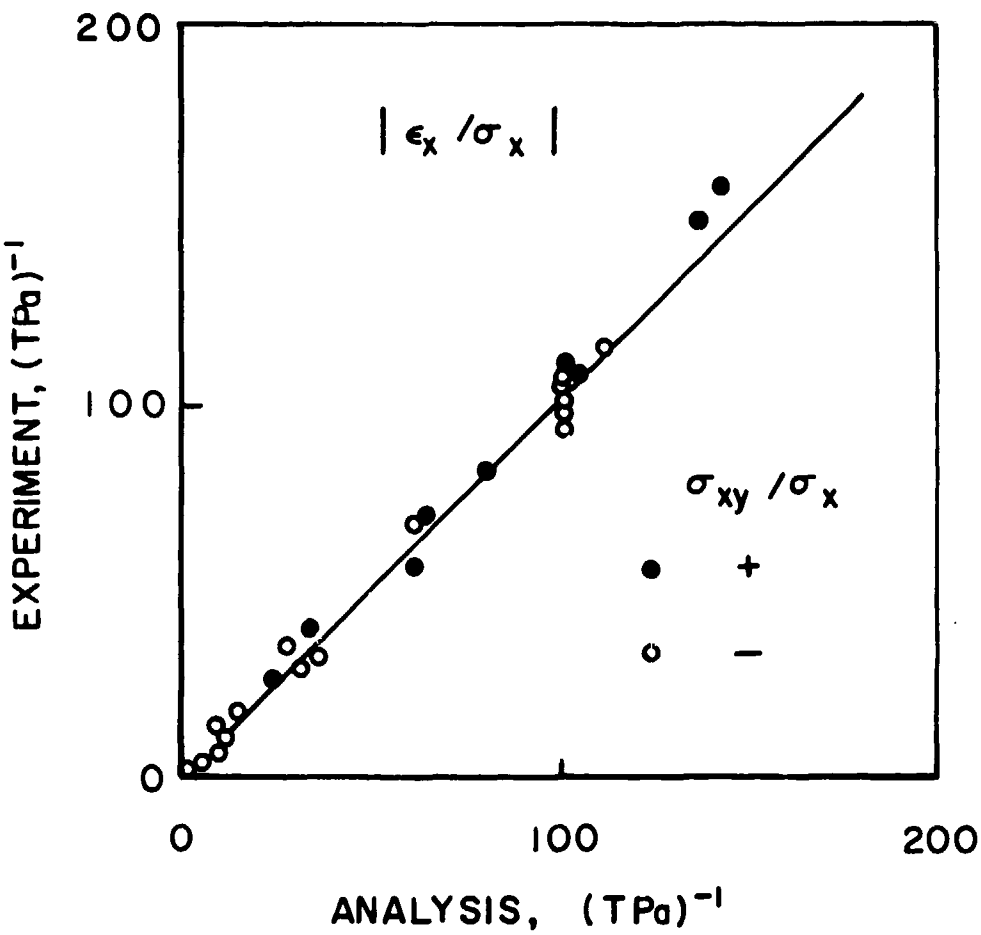

Figure 10. Analysis-Experiment Correlation:
(a) $|e_x/\sigma_x|$

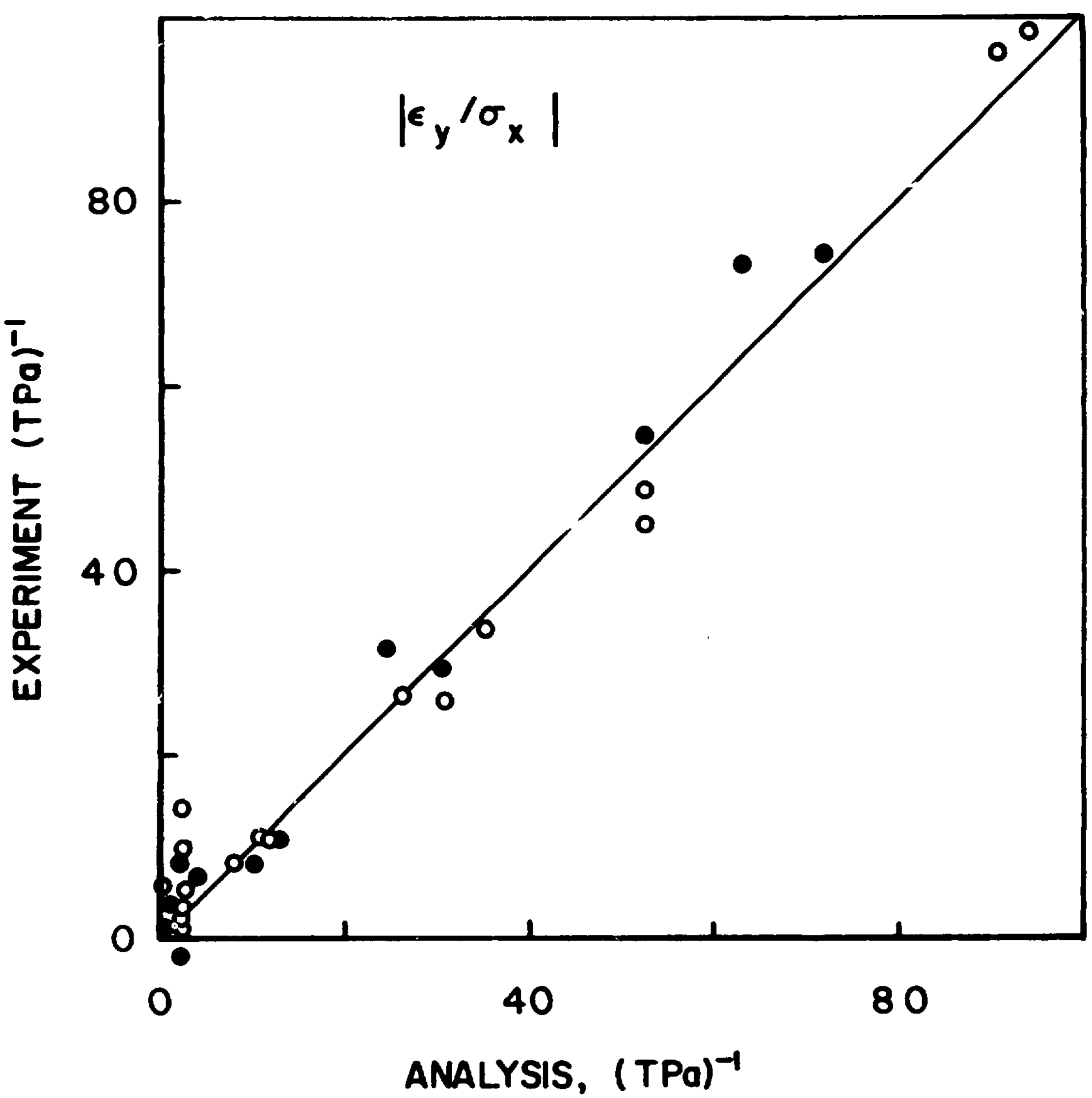

Figure 10(b). $|\epsilon_y/\sigma_x|$

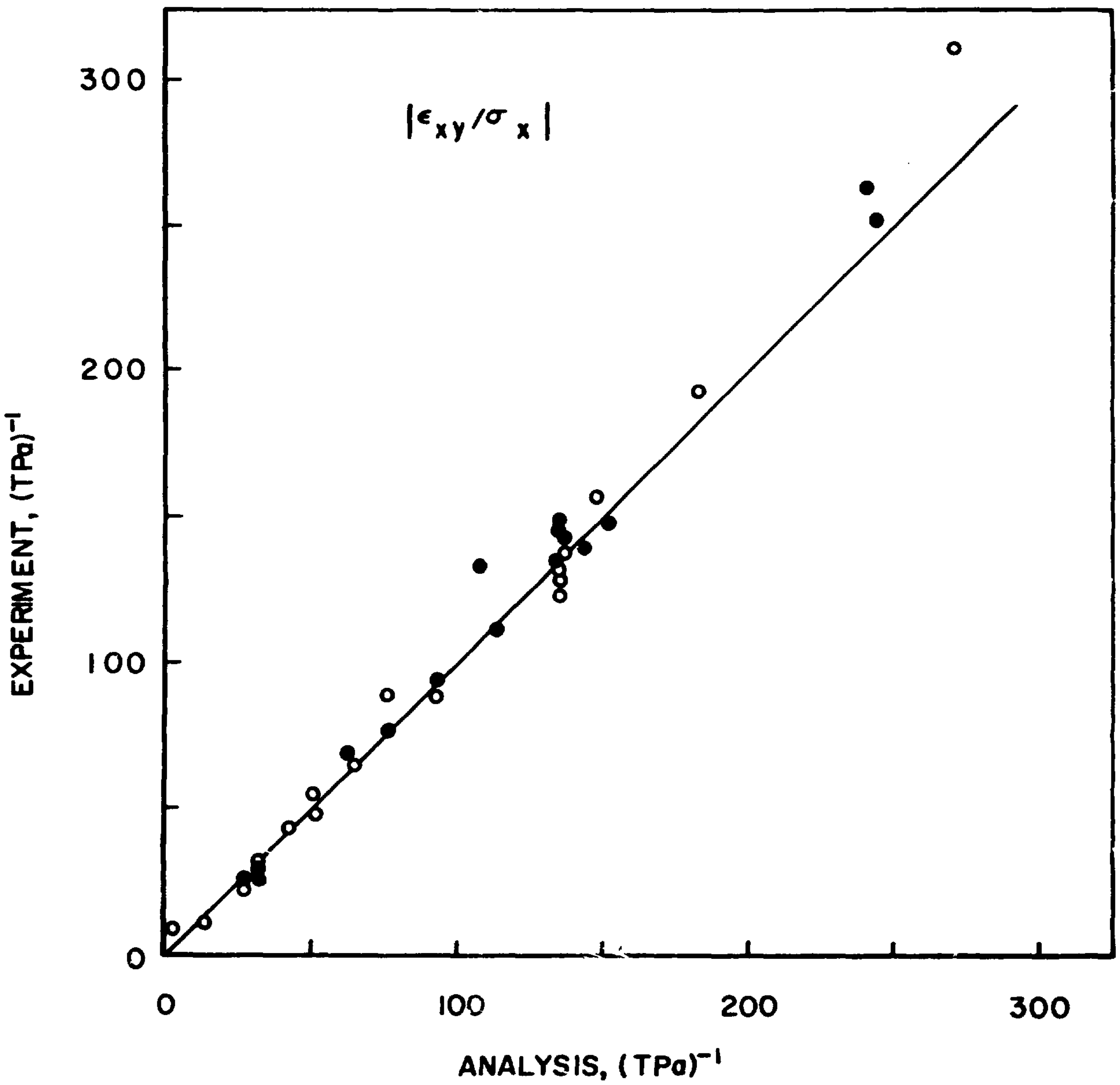

Figure 10(c). $|e_{xy}/\sigma_x|$

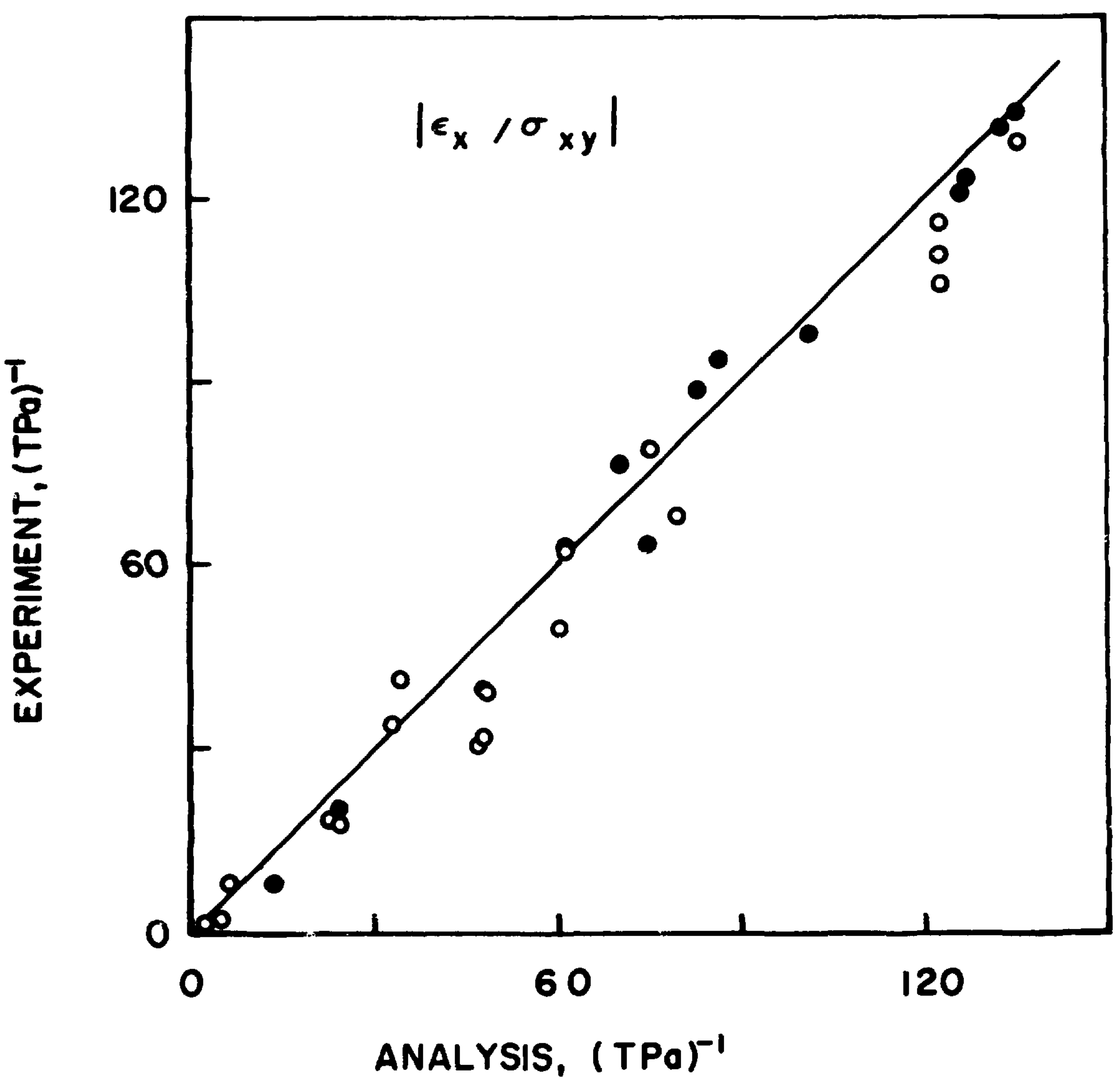

Figure 10(d). $|\epsilon_x/\sigma_{xy}|$

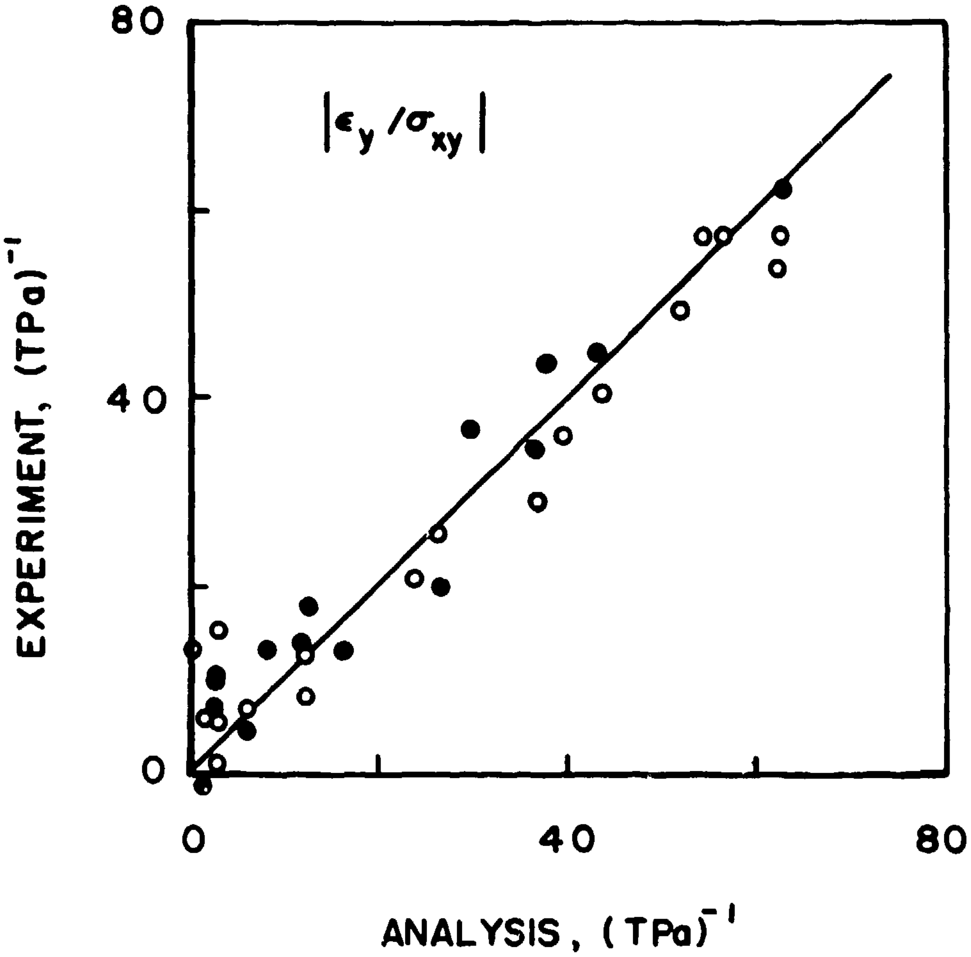

Figure 10(e). $|\epsilon_y/\sigma_{xy}|$

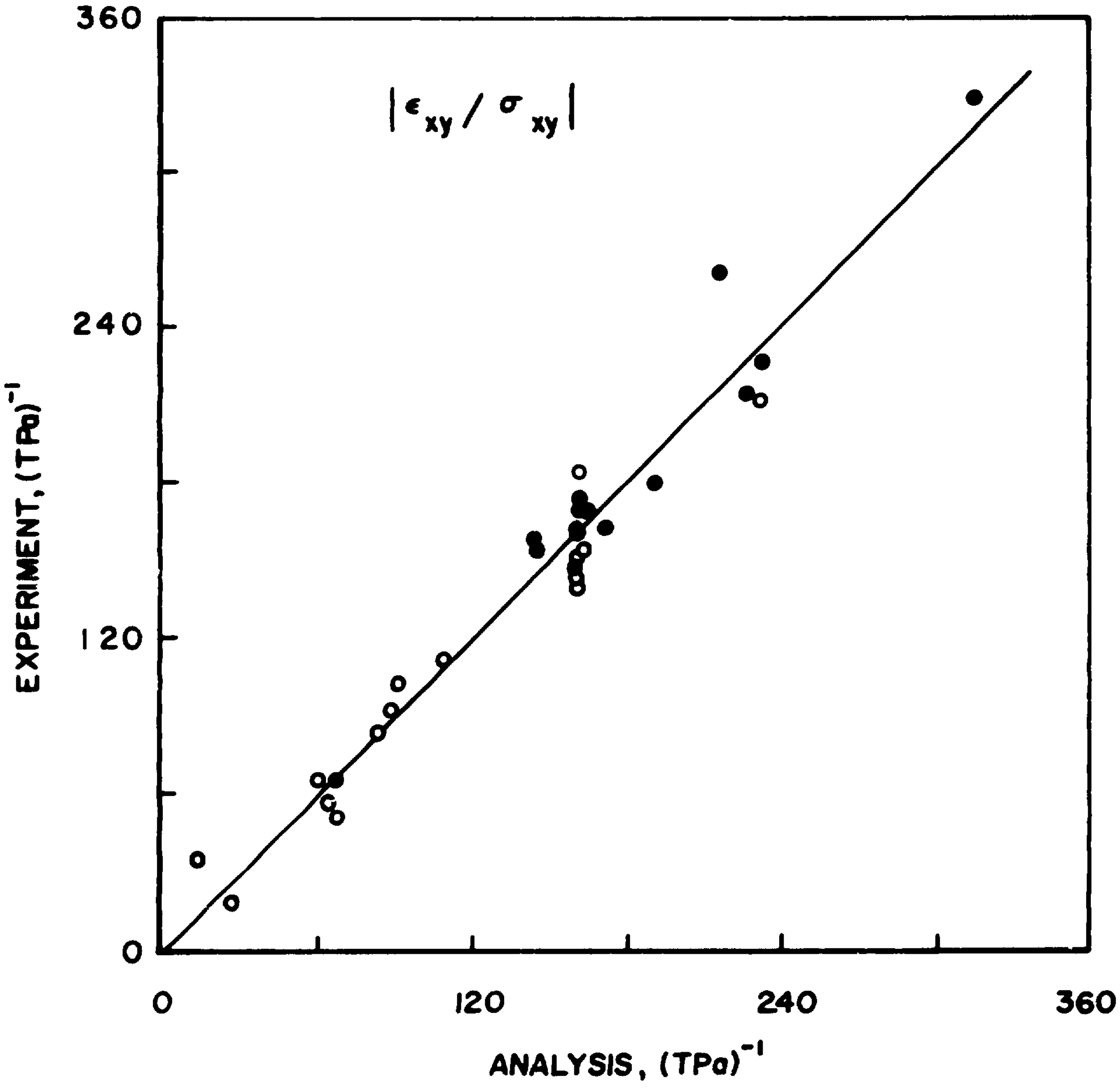

Figure 10(f). $|\epsilon_{xy}/\sigma_{xy}|$

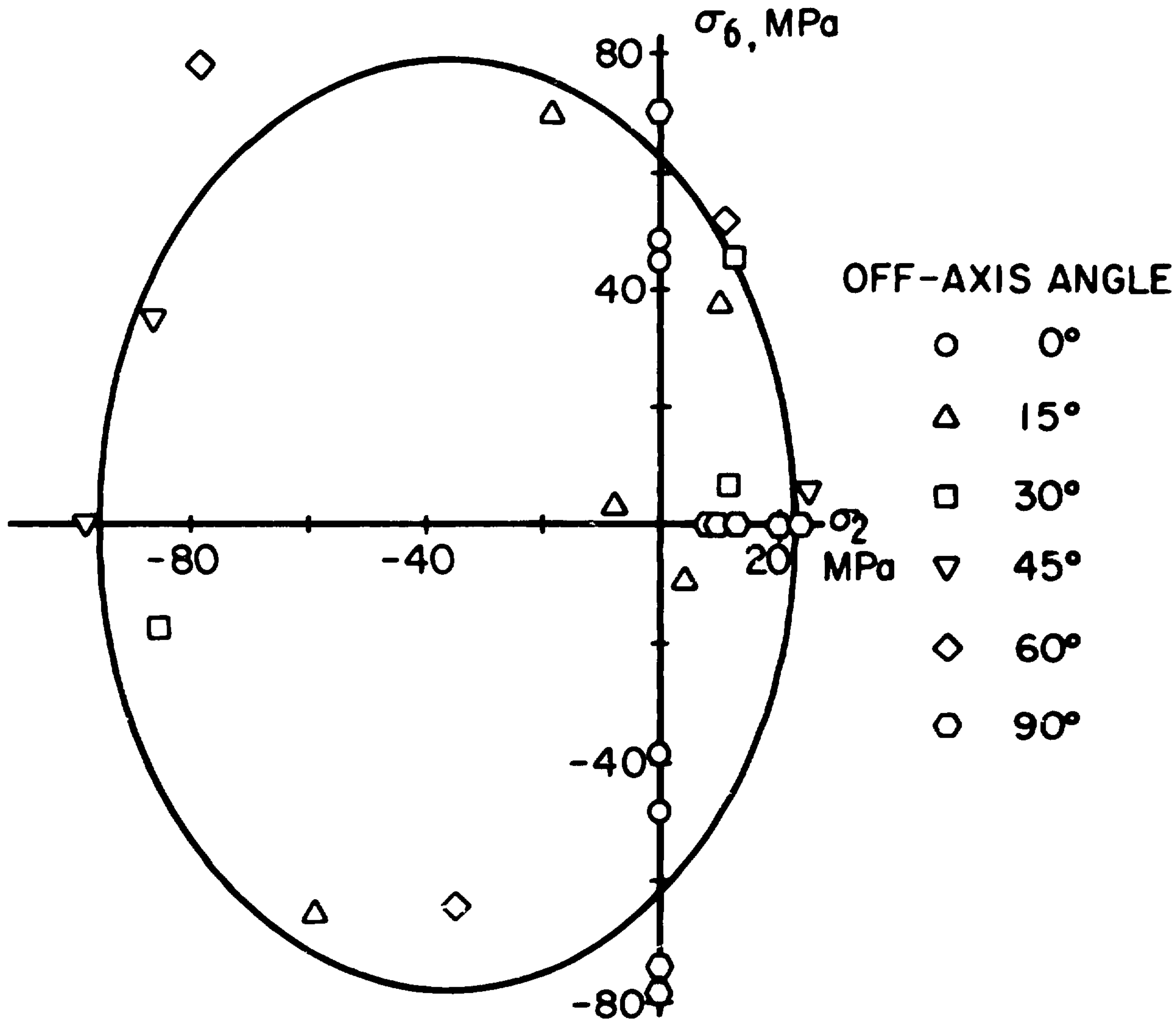

Figure 11. Failure Surface in σ_2 - σ_6 Plane

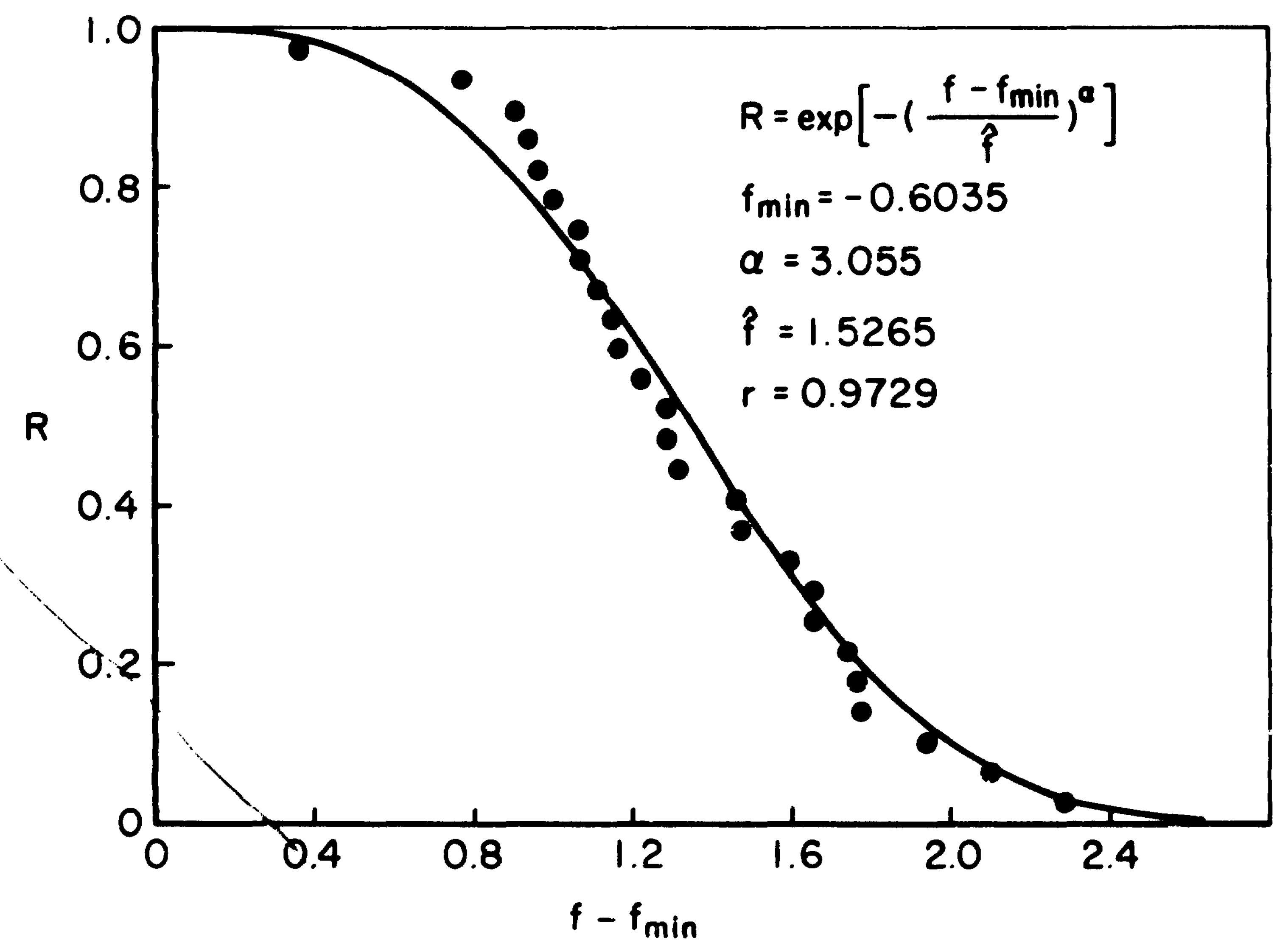

Figure 12. Distribution of f

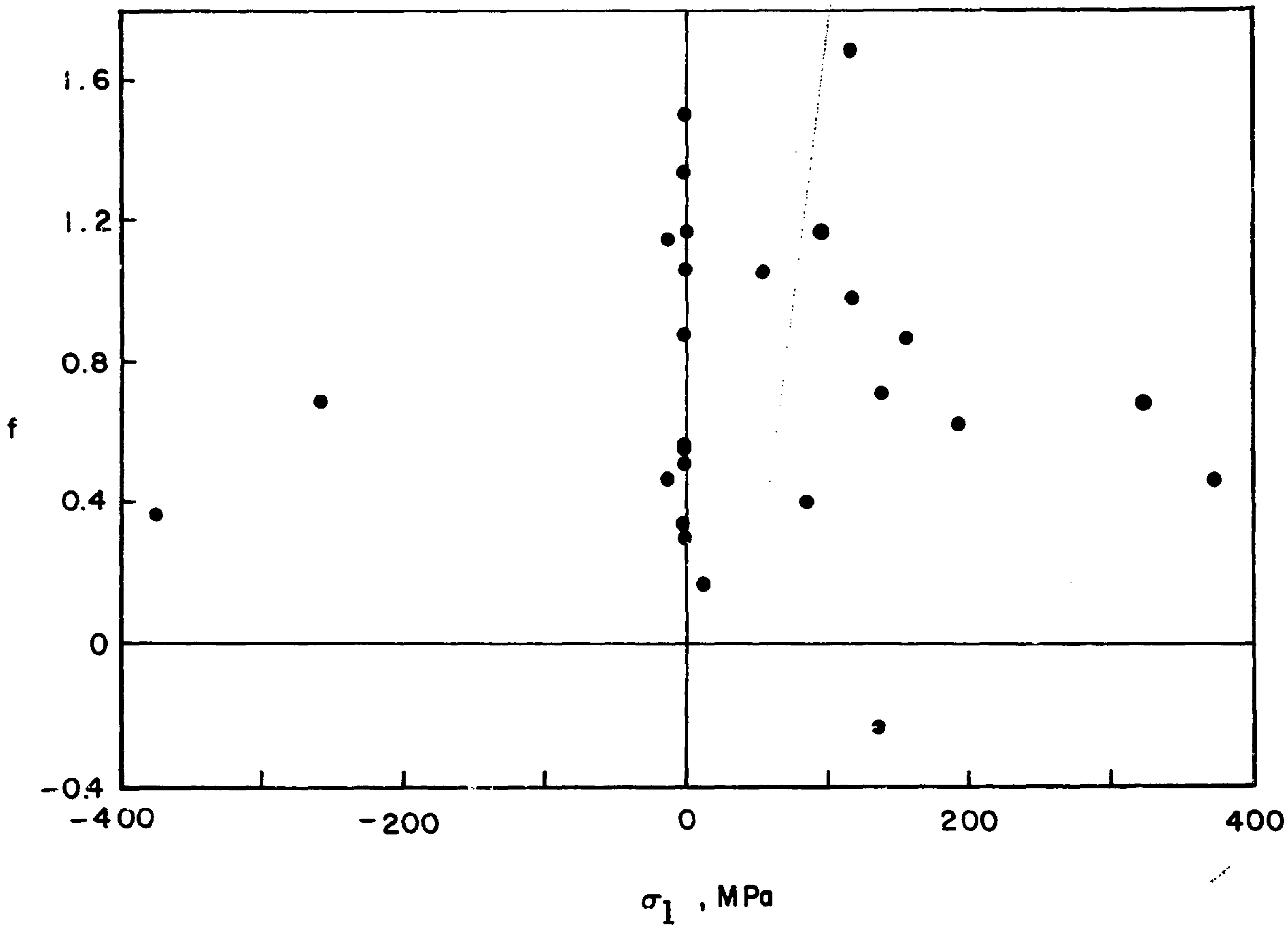

Figure 13. Effect of Longitudinal Stress on f

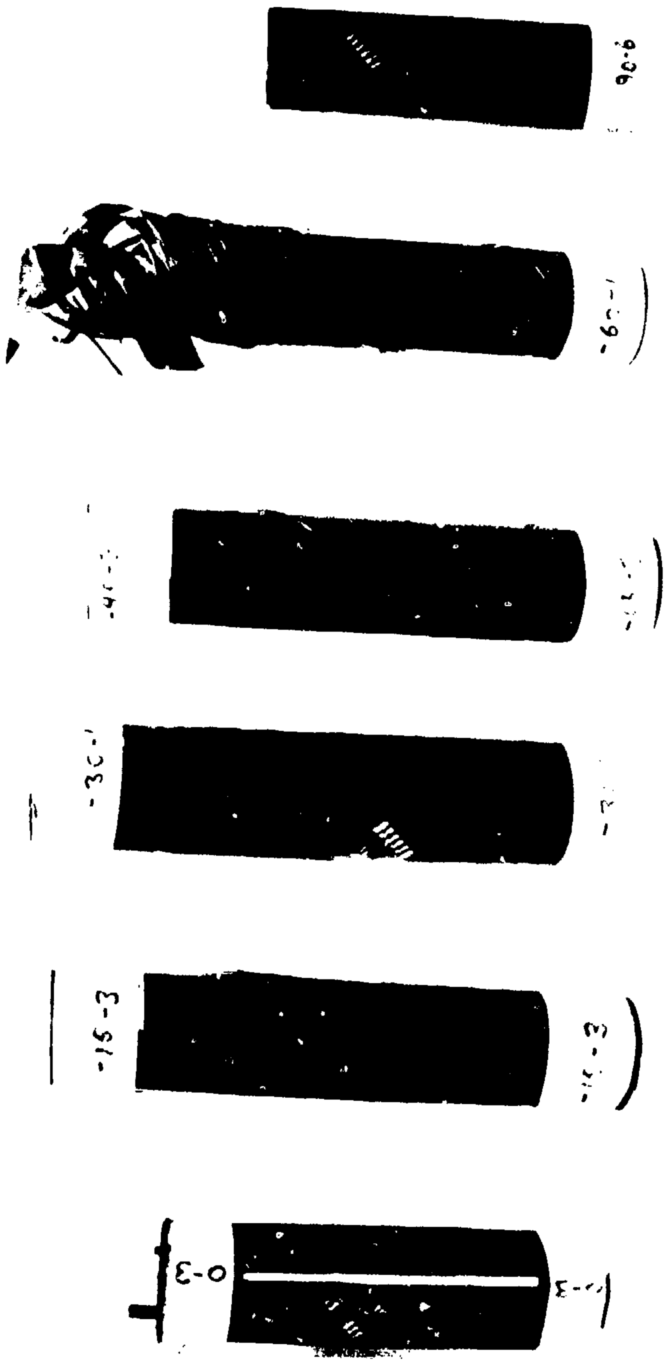

Figure 14. Failure Modes of Composite Tubes

☆U.S.Government Printing Office: 1977 — 757-080/279